Programmed knockout mutation of liver fluke granulin, *Ov-grn-1*, impedes malignant transformation during chronic opisthorchiasis

Sujittra Chaiyadet[1, 2, 3] Sirikachorn Tangkawattana[3,4], Michael J Smout[3,5,], Wannaporn Ittiprasert[3,6], Victoria H. Mann[6], Raksawan Deenonpoe[7], Patpicha Arunsan[1,6], Alex Loukas[5,8], Paul J Brindley[6, 8], Thewarach Laha[1,8]

[1] Department of Parasitology, Faculty of Medicine, Khon Kaen University, Khon Kaen, 40002 Thailand

[2] Tropical Medicine Graduate Program, Academic Affairs, Department of Parasitology, Faculty of Medicine, Khon Kaen University, Khon Kaen, 40002 Thailand

[3]equal contribution

[4] Faculty of Veterinary Medicine, Khon Kaen University, Khon Kaen, Thailand, and WHO Collaborating Center for Research and Control of Opisthorchiasis, Tropical Disease Research Center, Khon Kaen University, Khon Kaen 40002, Thailand

[5] Centre for Molecular Therapeutics, Australian Institute of Tropical Health and Medicine, James Cook University, Cairns, Queensland, 4878, Australia

[6] Department of Microbiology, Immunology and Tropical Medicine, and Research Center for Neglected Diseases of Poverty, School of Medicine & Health Sciences, George Washington University, Washington, D.C. 20037, USA

[7]Department of Pathology, Faculty of Medicine, Khon Kaen University, Khon Kaen, 40002 Thailand

[8]correspondence: Thewarach Laha, email, thewa_la@kku.ac.th; Alex Loukas, email, alex.loukas@jcu.edu.au; Paul Brindley, email, pbrindley@gwu.edu

Abstract

Infection with the food-borne liver fluke *Opisthorchis viverrini* is the principal risk factor for cholangiocarcinoma in the Mekong Basin countries of Thailand, Lao PDR, Vietnam, Myanmar and Cambodia. Using a novel model of CCA, involving infection with gene-edited liver flukes in the hamster during concurrent exposure to a nitrosamine, we explored the role of the fluke granulin-like growth factor *Ov*-GRN-1 in malignancy. We produced programmed gene knockout flukes (*ΔOv-grn-1)* by delivery of a CRISPR/Cas9/gRNA system by electroporation. Genome sequencing confirmed Cas9-catalyzed mutations in the targeted genes, which was accompanied by rapid depletion of transcripts and the cognate proteins. Whereas *Ov-grn-1* gene-edited parasites colonized the biliary tract and developed into adult flukes, less hepatobiliary tract disease manifested during chronic infection with *ΔOv-grn-1* worms in comparison to hamsters infected with control parasites. Specifically, immunohistochemical analysis of thin sections of livers revealed markedly less periductal fibrosis surrounding the flukes and less liver fibrosis globally during infection with *ΔOv-grn-1* genotype worms, minimal biliary epithelial cell proliferation, and markedly fewer mutations of *TP53* in biliary epithelial cells. Moreover, fewer hamsters developed high-grade cholangiocarcinoma when infected with the *ΔOv-grn-1* flukes compared to controls. The clinically-relevant, pathophysiological phenotype of the hepatobiliary tract confirmed a role for this secreted growth factor in malignancy and morbidity during opisthorchiasis.

Keywords
Infection-associated cancer; liver fluke; opisthorchiasis; cholangiocarcinoma; CRISPR/Cas; knockout; granulin

Introduction

Liver fluke infection caused by species of *Opisthorchis* remains a major public health problem in East Asia and Eastern Europe. Infection with *O. viverrini* is endemic in Thailand and Laos, where ~10 million people are infected with the parasite. Opisthorchiasis is associated with hepatobiliary diseases including cholangiocarcinoma [1], or bile duct cancer [2]. Northeast Thailand reports the world's highest incidence of CCA, >80 per 100,000 in some provinces. No stronger link between malignancy and a parasitic infection occurs than that between CCA and *O. viverrini*. Indeed, the International Agency for Research on Cancer of the World Health Organization classifies infection with *O. viverrini* as a Group 1 carcinogen, i.e. definitely carcinogenic in humans [2-4].

The mechanism by which opisthorchiasis induces CCA is likely multi-factorial, including mechanical irritation of the biliary tract during migration and feeding of the liver fluke, metabolites released by the parasite, and nitrosamines in fermented foods that are a dietary staple in countries of the Mekong River basin. To survive in hostile environs, parasitic helminths excrete and secrete a battery of proteins (excretory/secretory proteins [ES]) and other mediators with diverse effects and roles at the host–parasite interface. This interaction has long been thought to manipulate host cellular homeostasis and underwrite malignant transformation during chronic opisthorchiasis, but the molecular mechanisms by which these processes occur are poorly understood. Focusing on the ES contribution to carcinogenesis, we here targeted the growth factor *Ov*-GRN-1, *O. viverrini* granulin, one component of the ES complement that we have determined induces phenotypic hallmarks of cancer [5]. We have reported that *Ov*-GRN-1 and other ES components including extracellular vesicles (EVs) enter cholangiocytes, the epithelial cells that line the biliary tract, and drive cellular signaling that can promote carcinogenesis, including cellular proliferation and migration, angiogenesis and wound healing [6]. Also, we recently confirmed the role of *Ov*-GRN-1 in driving proliferation of bile duct epithelial cells (cholangiocytes) by genetic manipulation of its expression in the liver fluke both by RNAi and by CRISPR/Cas9 gene editing [7]. Moreover, we have shown that infection of hamsters with gene edited infectious fluke larvae is feasible and, shown that proliferation of biliary epithelia is markedly suppressed during infection with the *Ov-grn-1-/-* (*ΔOv-grn-1*) flukes.

There is an established, tractable model of induction of CCA in experimentally infected hamsters, where 100% of hamsters infected with metacercariae of the parasite and exposed to otherwise sub-carcinogenic levels of dietary dimethyl nitrosamine (DMN) develop CCA within a few months after infection with the liver fluke [8-10]. In the Syrian golden hamster, *O. viverrini* infection causes periductal fibrosis. Severe periductal fibrosis induced by the parasite combined with a nitric oxide carcinogen, such as DMN, results in epithelial hyperplasia, cholangiocyte proliferation and DNA damage, eventually culminating in CCA in hamsters [11]. Here, we investigated the effect of infection of hamsters with *O. viverrini* following programmed knock out the *Ov-grn-1* gene in the infective stage of the liver fluke before experimental infection of hamsters in relation to fluke induced periductal fibrosis and malignant transformation of the hepatobiliary tract. Immunohistochemical analysis of thin sections of hamster livers revealed markedly less fibrosis during infection with *ΔOv-grn-1* worms, minimal cholangiocyte proliferation, substantially less expression of mutant p53 tumor protein, and diminished

malignancy of the hepatobiliary tract. The clinically-relevant, pathophysiological phenotype of the livers of the hamsters confirmed a role for this parasite secreted growth factor in morbidity and malignancy during opisthorchiasis, and highlight the tractability of CRISPR/Cas9 for addressing gene function in flatworms.

Results

Programmed CRISPR/Cas-9 knock-out of genes of *O. viverrini*

To investigate the effect of programmed gene knock-out in *O. viverrini*, hamsters were infected with NEJs of *O. viverrini* that had been subjected to CRISPR/Cas genome editing. The C CRISPR/Cas systems were delivered by electroporation of plasmids encoding guide RNAs specific for *Ov-grn-1* or *Ov-tsp-2* or a control (scramble - SCR) guide RNA and Cas9 of *S. pyogenes*. Figure 1A summarizes the experimental approach and timelines, the findings from which are presented below.

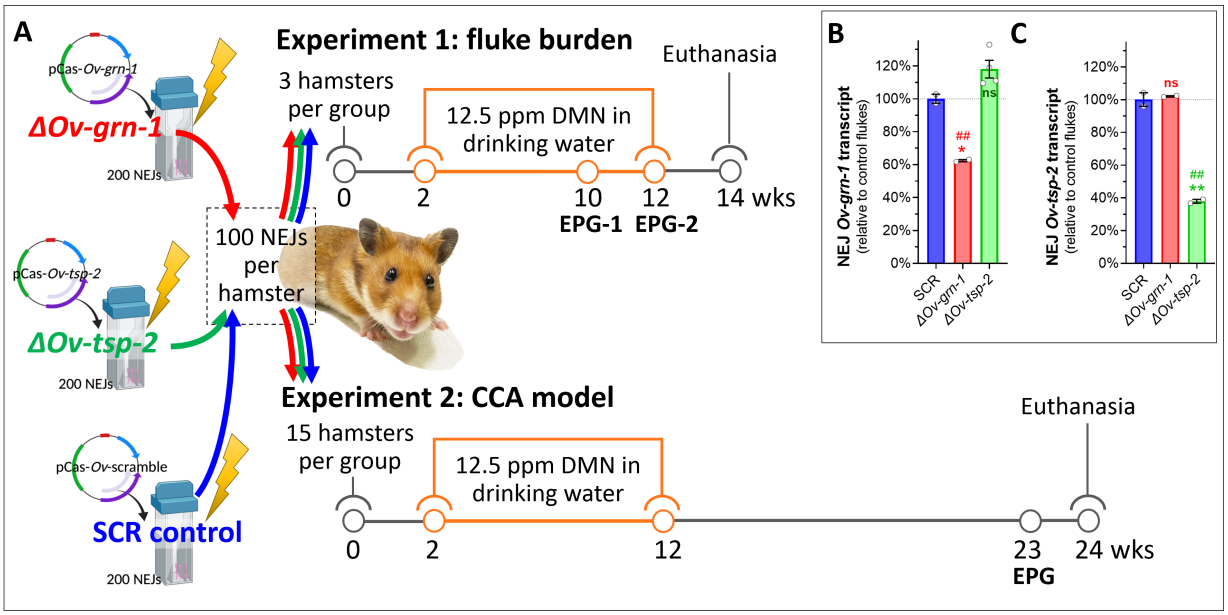

***Figure 1. Experimental designs**. Hamsters were infected with gene edited or control flukes for 14 weeks to assess the impact of CRISPR/Cas9 editing on fluke survival (panel **A**) or 24 weeks to assess the impact of CRISPR/Cas9 editing on pathogenesis including CCA (**B**). Each experiment had three groups of hamsters infected with flukes treated with CRISPR/Cas9 plasmids targeting either Ov-grn-1 (red: ΔOv-grn-1), Ov-tsp-2 (green: ΔOv-tsp-2), or a scrambled control (blue: SCR) designed to not match any O. viverrini sequence. For both experiments two hundred newly excysted juveniles (NEJ) per cuvette were transfected with 10 µg of CRISPR-Cas9 plasmid via electroporation (lightning bolt). Each hamster was infected with 100 NEJs by stomach intubation After 2 weeks, the hamsters were supplied 12.5 ppm dimethyl nitrosamine (DMN) in drinking water for 10 weeks to accelerate carcinogenesis. In experiment 1, eggs per gram of feces (EPG) was determined at 10 and 12 weeks and the hamsters euthanized at week 14 of infection. In experiment 2, EPG was assessed at week 23 followed by euthanasia at week 24. Transcript levels in edited NEJs of Ov-grn-1 (B) and Ov-tsp-2 (C) were assessed by qPCR. To monitor programmed gene knockout, the gene transcript levels in 200 pooled NEJs were determined with 2-4*

148 *biological qPCR replicates and were plotted relative to 100% SCR control transcript levels. Each*
149 *targeted gene shows significant transcript reduction in the relevant group, while the non-targeted gene*
150 *shows no significant change to the SCR transcript level. Comparing each group with one-way ANOVA*
151 *with Holm-Sidak multiple comparison against SCR control: ns = not significant; *, P ≤ 0.05; **, P≤*
152 *0.01; ΔOv-grn-1 vs ΔOv-tsp-2, ##, P≤ 0.01.* .

153 Changes in transcription of the targeted genes that would reflect programmed genomic changes
154 were monitored by RT-qPCR. Relative to the SCR group, the *Ov-grn-1* transcript levels were
155 significantly reduced in the *ΔOv-grn-1* flukes by 37.6% (P<0.05) whereas the transcription of
156 *Ov-tsp-2* was not significantly changed in the *ΔOv-grn-1* flukes (18%, *ns*) (Figure 1B).
157 Transcription of *Ov-tsp-2* was significantly reduced in the *ΔOv-tsp-2* flukes (62.1%; P<0.01)
158 whereas the levels of *Ov-grn-1* transcripts were not significantly changed (Figure 1C). These
159 findings indicated on-target gene knockout at both the *Ov-grn-1* and *Ov-tsp-2* loci.
160
161 **Effect of CRISPR/Cas-9 targeted mutation of *Ov-grn-1* or *Ov-tsp-2* on adult flukes**
162
163 In experiment 1, feces were sampled from each hamster at both 10 and 12 weeks after infection.
164 Significant differences in fecal eggs (EPG) were not apparent among the three groups at these
165 timepoints (Figure 2A). Hamsters were euthanized and necropsied at 14 weeks to investigate the
166 numbers of adult *O. viverrini* in the hepatobiliary tract. The numbers of worms in the control
167 SCR, *ΔOv-grn-1*, and *ΔOv-tsp*-2 groups were 60.0±3.46 (mean ± SEM), 36.7±3.48, and
168 21.3±2.96, reflecting reductions of 38.9% and 64.5%, respectively, compared to the SCR control
169 group (Figure 2B).
170
171 Of the worms recovered from the livers, 10-13 from each of the three hamsters in each group
172 were evaluated by RT qPCR for gene transcript levels relative to the SRC (control) flukes.
173 Transcipt levels of both genes expressed by the control SCR parasites were generally clustered
174 around 100% (Figure 2C, D). Transcript levels for *Ov-grn-1* ranged broadly in the Δ*Ov-grn-1*
175 flukes but were significantly reduced by 54% compared to the SCR group (Figure 2C; P≤ 0.001).
176 This broad range, 100 – 0%, in *Ov-grn-1* transcript levels was similar to the findings in our
177 earlier report [7]. The outcome, where most flukes either not showing a change (~100%) or, by
178 contrast, showing a near absence of transcription (~0%) was not normally distributed, which
179 required a non-parametric statistical approach. Median values were reported for these analyses.
180 In contrast to the NEJ, which showed substantial knockdown of *Ov-tsp*-2 (Figure 1), the adult
181 stage *ΔOv-tsp*-2 flukes showed only a modest reduction in transcript levels (9%) compared to the
182 SCR group (Figure 2D). Although transcript levels for *Ov-tsp*-2 were significantly reduced (P≤
183 0.01*),* they generally showed minimal change with two individual flukes only exhibiting > 50%
184 reduction in expression. This marked difference, when compared to transcript levels for *Ov-tsp*-2
185 in NEJ -- reduced by 62.1%, in addition to the reduction by 65% of numbers of worms recovered
186 at necropsy, indicated that *Ov-tsp-2* gene knockout lead to a lethal phenotype and that flukes of
187 this genotype failed to survive *in vivo*. This contrasted with programmed knockout of *Ov-grn-1*
188 where the majority of flukes of the Δ*Ov-grn-1* genotype survived even though transcription of
189 *Ov-grn-1* was not detected in four of 36 flukes and 10 of 36 exhibited *Ov-grn-1* transcript levels
190 <5% of those expressed in the control group worms.

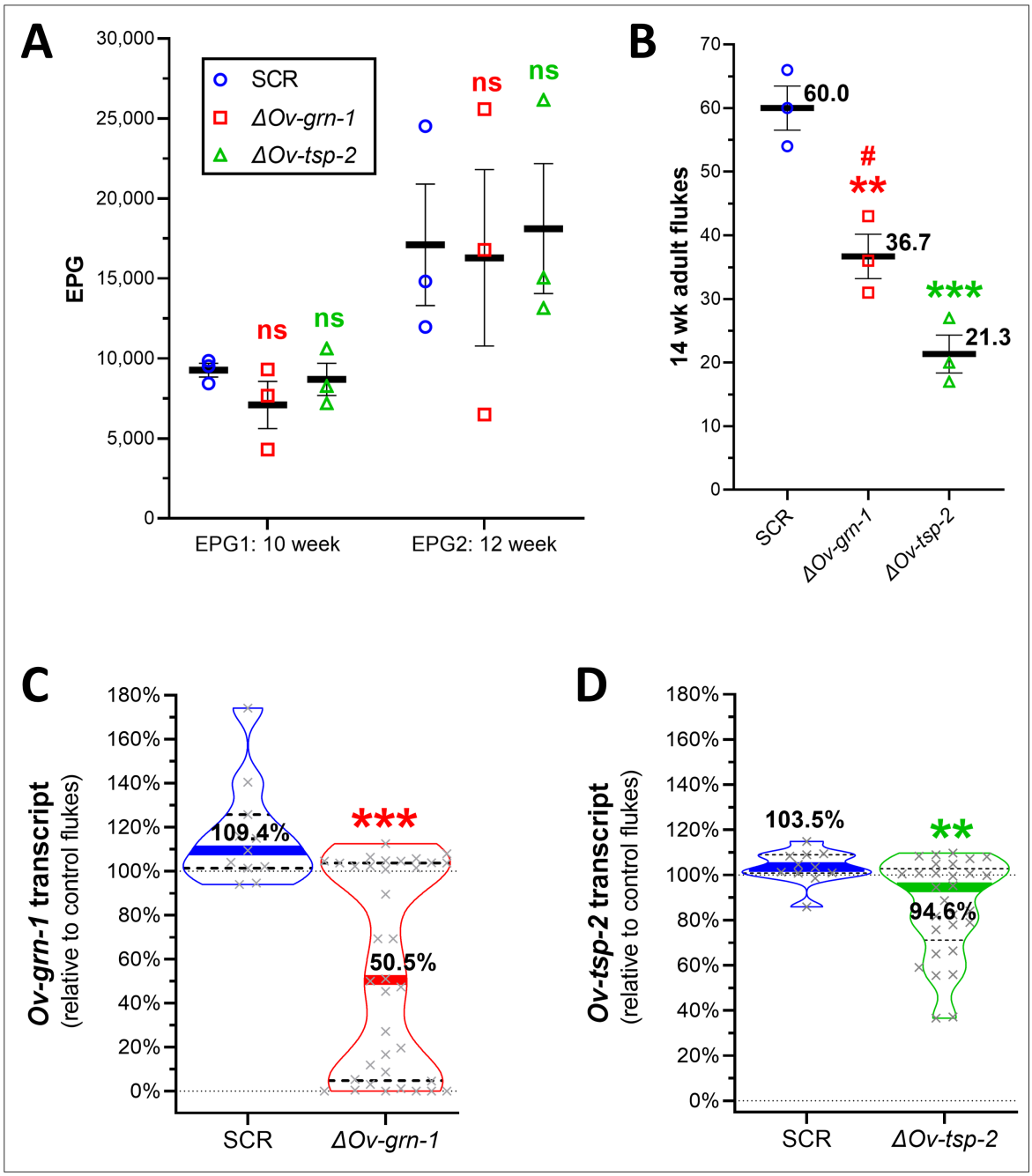

Figure 2. Liver fluke burden and levels of gene transcription. *Fluke fecundity, adult fluke numbers, and gene expression levels were determined at 10-14 weeks* ***(****experiment 1****)*** *with 100 gene edited NEJs per hamster, and from three hamsters per group.* *Number of eggs per gram of feces* ***(****EPG****)*** *from each hamster at weeks 10 and 12* ***(A)*** *and fluke burden at week 14* ***(B)*** *showing average* ***(****horizonal black line****)*** *and SEM bars.* *Each treatment group was compared against matched SCR control with 2-way ANOVA with Holm-Sidak multiple comparison: ns = not significant;* *****,*** *P≤ 0.01;* ******,*** *P<0.001, and against ΔOv-tsp-2:* ***#*** *, P≤ 0.05.* *A total of 10-12 flukes per animal were processed for qPCR to determine gene transcript levels of* Ov-grn-1 ***(C)*** and Ov-tsp-2 ***(D)*** *and plotted as violin plots with each data point representing the transcript level of individual flukes relative to control flukes; median denoted by thick colored line and quartiles by the black line.* *The distribution was non-parametric and subsequently the*

202 *two-tailed Mann-Whitney* t *test was used to compare transcript levels with those of the SCR control;* ***,
203 P≤ *0.01;* ***, P≤ *0.001 for each gene.*

204 **Parasitological impact of CRISPR/Cas-9 gene knockout**
205

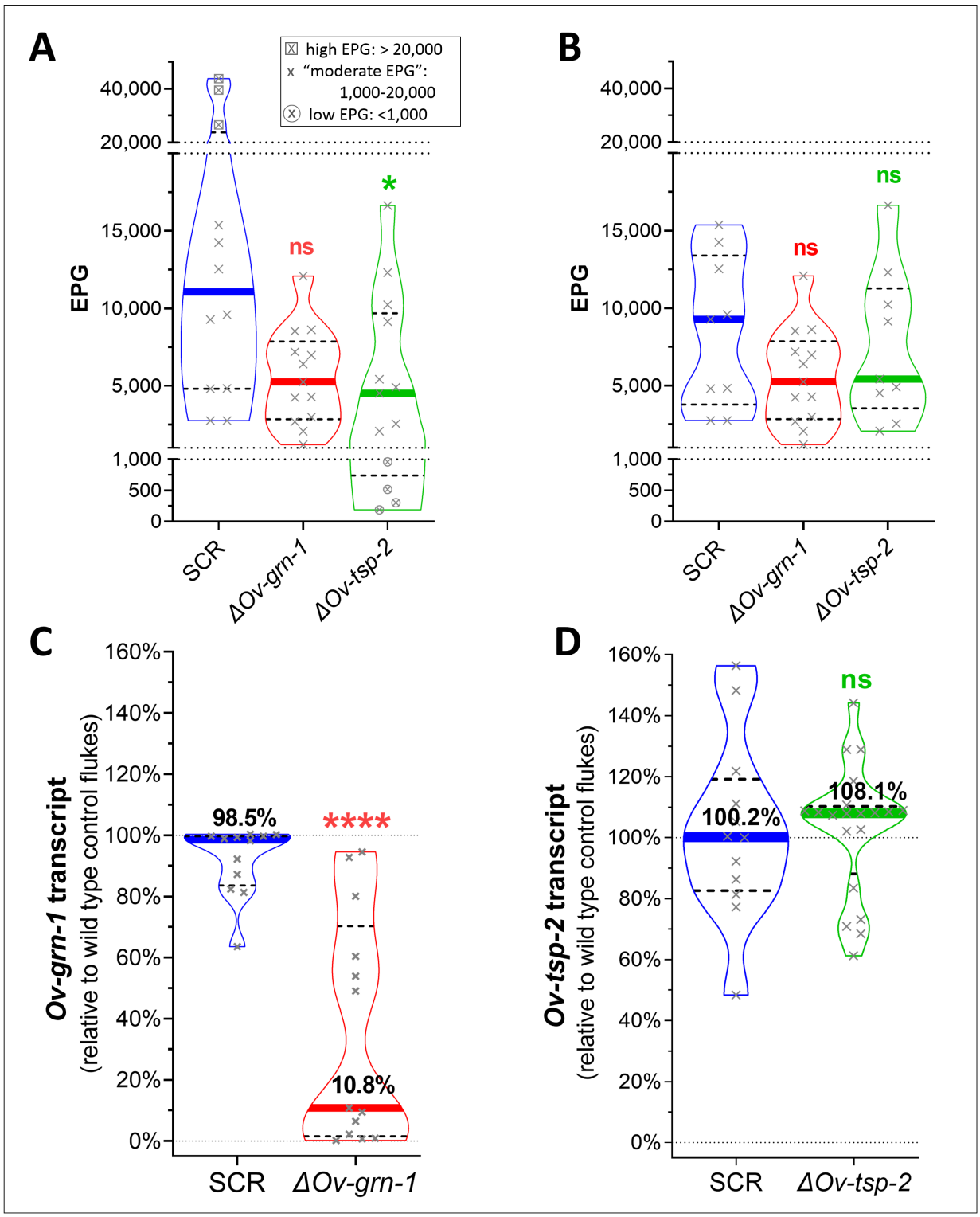

206
207

Figure 3*. Cholangiocarcinoma model, fecundity, and gene transcript and mutation rates.** *Eggs per gram of feces (EPG) was assessed at week 23 prior to euthanasia at week 24 (experiment 2). Panel A shows the EPG of the three groups of all hamsters. Violin plot denotes each animal's EPG with "x" symbols. Circle enclosed "x", (ⓧ), signifies animals with low EPG below 1,000 and square enclosed "x", (☒), signifies animals with high EPG above 20,000. Solid colored lines indicate the median values and dashed black lines indicate the quartiles.* ***B *shows the same EPG with low/high animals removed, these "moderate EPG" animals had 1,000-20,000 EPG. The distribution was non-parametric and subsequently the Kruskal Wallis with Dunn's multiple comparison correction was used to compare EPG levels against SCR control: *, P <0.05; ns = not significant. At week 24, hamsters were euthanized, 12-20 flukes collected from each group and transcript levels determined of Ov-grn-1* ***(C)*** *or Ov-tsp-2* ***(D)****. Violin plots are shown with each data point representing the transcript level for individual flukes relative to control flukes. The thick solid line is the median and the dashed black lines are the inter-quartile ranges.* ***C, D****, Mann-Whitney non-parametric t-test comparing transcript levels against SCR control for each gene: ns, not significant;* ****, P ≤ 0.0001.*

A primary goal for experiment 2 was the histopathological and histochemical assessment of hepatobiliary disease at 24 weeks of infection. Accordingly, determining the number of surviving liver flukes was not feasible because the liver and its intrahepatic biliary tract, occupied by the parasites, was fixed in formalin at necropsy. However, a sample of the resident *O. viverrini* were collected, to screen for efficacy of CRISPR/Cas9 gene knockout, before formalin fixation of the the liver. In lieu of counting the number of worms parasitizing each hamster, fecal egg count (as eggs per gram of feces, EPG) were determined at the time of necropsy. Numbers of eggs of *O. viverrini* positively correlate with number of worms within the hepatobiliary tract [12, 13]. There was a broad range of EPG values among all the groups (Figure 3A) although feces of the SCR fluke infected hamsters had the highest EPG values, median =11,062 EPG, the *ΔOv-grn-1* group, 5,267 EPG, and the *ΔOv-tsp-2* group 4,530 EPG ($P \leq 0.05$), reflecting the same rank order in numbers of worms recovered from these groups (Fig. 2B, experiment 1). Although the number of fecal eggs correlates positively with numbers of worms during infection with *O. viverrini* [13], the variations in numbers of flukes among the groups, as predicted from the EPG values, confounds comparisons of the corresponding pathogenesis and lesions. Hence, to mitigate the impact of variations in numbers of liver flukes on the analysis and interpretation of the role of gene knockout on hepatobiliary disease and malignancy, the histopathological assessments focused on the livers of hamsters with "moderate" EPG values, i.e. *ΔOv-grn-1* EPG ranging from 1,000 to 20,000 (Figure 3A, B, dotted lines). This cutoff window excluded three SCR hamsters with values of 26,000 to 44,000 EPG and four *ΔOv-tsp*-2-infected hamsters with ≤ 1,000 EPG. Figure 3B shows the "moderate EPG" values with 9,279 EPG in SCR-, 5,267 in Δ*Ov-grn-1*- and 5,434 in *ΔOv-tsp-2*-fluke infected hamsters with overlapping inter-quartile ranges. Significant differences among the groups (within the cutoff window) were not apparent. Whereas the surviving flukes did not show changes in expression of *Ov-tsp*-2 (Figures 2D and 3D), the hamsters infected with *ΔOv-tsp*-2 parasites were included as a low fluke burden comparator. It was likely that fewer flukes survived in the *ΔOv-tsp*-2 group of hamsters, including those hamsters with comparable EPGs, (Figure 2A, B).

Adult worms recovered from hamster livers examined at 24 weeks after infection were evaluated for targeted gene transcripts by qPCR. Transcript levels of *Ov-grn-1* in adult *O. viverrini* from Δ*Ov-grn-1* infected hamsters were significantly decreased (89%, $P \leq 0.0001$) compared to the SCR control group (Figure 3C), whereas the *ΔOv-tsp-2* flukes showed a non-significant increase (8%) compared to the SCR group (Figure 3D). With experiments 1 and 2 showing the surviving

255 *ΔOv-tsp-2* worms expressing *Ov-tsp-2* at levels comparable to the control SCR flukes, we posit
256 that substantial *Ov-tsp-2* gene edits were lethal, and worms that survived to maturity likely had
257 not undergone gene editing and/or few of the cells in the worms had been edited. Although we
258 retained the *ΔOv-tsp-2* group for comparison of pathogenesis, the genotype of the flukes from
259 this group was not investigated further by targeted amplicon NGS.
260
261 **Synopsis of outcomes of CRISPR/Cas9 gene editing of the liver flukes**
262
263 To characterize mutations from the programmed knockouts, a region of 173 bp region flanking
264 the programmed cleavage site in *Ov-grn-1* was investigated by analyzing reads from targeted
265 amplicon NGS and analysis of the reads with CRISPresso2 [14]. Substitution patterns as
266 determined by the CRISPR-sub tool [15] in reads in the knockout groups were not significantly
267 different from the cognate alleles in the control SCR group worms (Figure S1). Also, we
268 scanned insertions and deletions (indels) and, in turn, the potential impact of indels on the open
269 reading frame. Figure 4A and Table S1 present the indel percentages of NEJs and adult flukes.
270 The Δ*Ov-grn-1* pooled NEJs showed 3.26% indel levels (2,723 of 80,571 reads), significantly
271 more than the 0.035% level in the SCR NEJ group (18 of 51,402 reads) ($P \leq 0.05$). The NEJ and
272 SCR adult flukes showed a similar indel % levels, with 0.045% in the adults (41 of 91,783
273 reads). Thirteen individual Δ*Ov-grn-1* adult liver flukes displayed a broad range of editing
274 efficiency in terms of indel profiles. These ranged from an apparent absence of programmed
275 mutation (no indels) to near complete gene knockout (91% indels), with a median of 3.1%
276 ($_{M}$Δ*Ov-grn-1*), which was significantly higher than in the SCR group flukes ($P \leq 0.01$). As noted
277 for levels of transcription, however, there were apparently distinct groupings of low mutation
278 flukes, six worms, (termed $_{L}$Δ*Ov-grn-1*) and six high mutation flukes ($_{H}$Δ*Ov-grn-1*) observed.
279 From a total of ~1.5 million NGS reads, programmed deletions (~0.5 million) were
280 overwhelmingly more common than insertions, seven of which seven were identified (Table S1).
281
282 The Δ*Ov-grn-1* indel percentage showed a strong inverse correlation with the transcript level
283 (Figure 4B), with a two-tailed non-parametric Spearman correlation co-efficient $r_s = -0.74$ ($P \leq$
284 0.01). The highly mutated, $_{H}$Δ*Ov-grn-1* flukes only minimally expressed the targeted *Ov-grn-1*
285 gene, <11% level of transcription of control SRC liver flukes. However, the highly edited
286 genotype/highly reduced transcription phenotype contrasted with the wide range of transcription
287 in the flukes with low or moderate levels of editing, $_{L}$Δ*Ov-grn-1* and $_{M}$Δ*Ov-grn-1,* with a wide
288 range of transcription from 6% to 94% of the levels of the control SRC group worms.
289
290
291
292
293
294
295
296
297
298
299
300

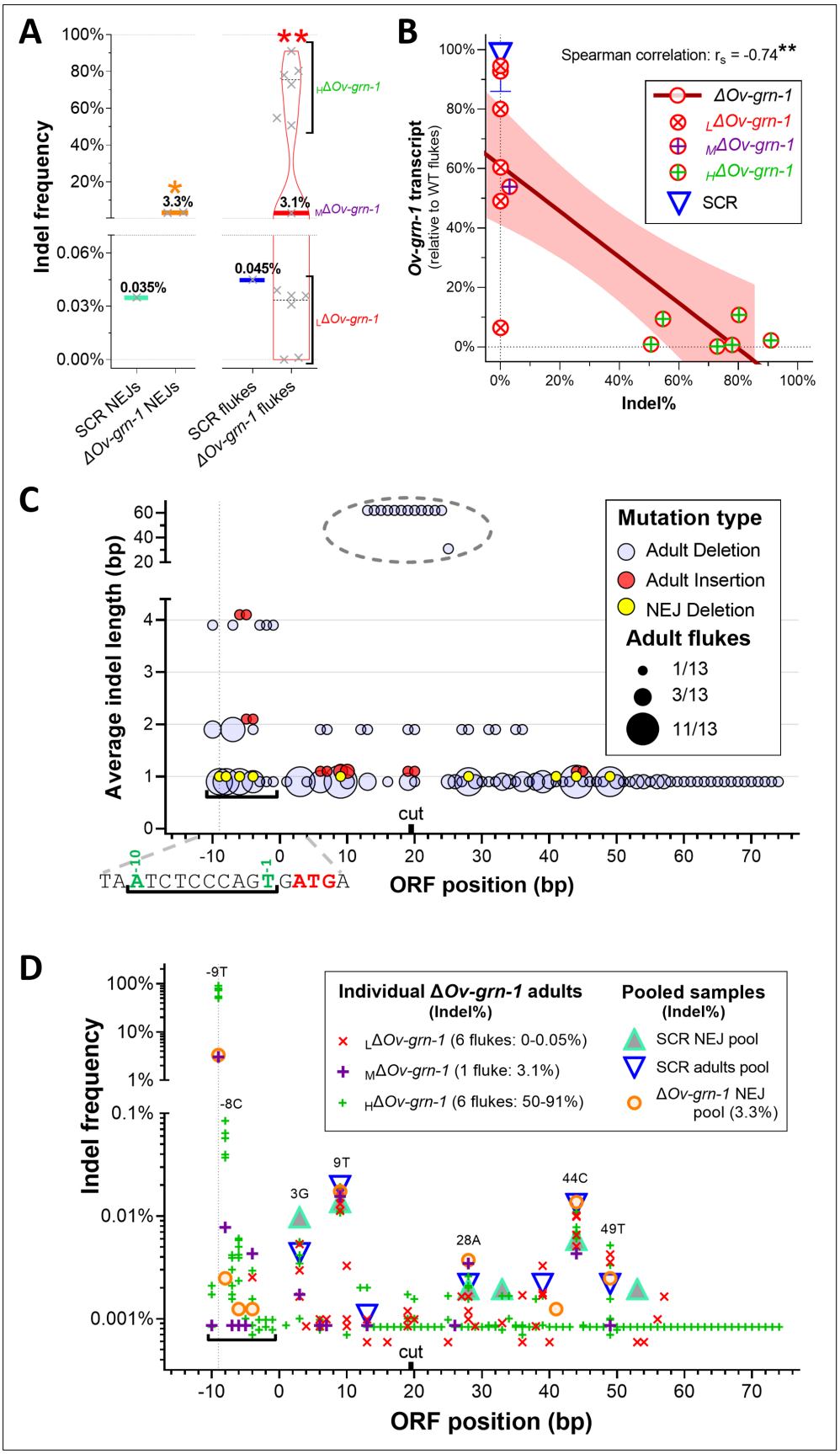
A
Indel frequency
100%
80%
60%
40%
20%
0.06%
0.03%
0.00%
3.3%
3.1%
0.035%
0.045%
**
*
HΔOv-grn-1
MΔOv-grn-1
LΔOv-grn-1
SCR NEJs
ΔOv-grn-1 NEJs
SCR flukes
ΔOv-grn-1 flukes
B
Spearman correlation: rs = -0.74**
Ov-grn-1 transcript
(relative to WT flukes)
Indel%
ΔOv-grn-1
LΔOv-grn-1
MΔOv-grn-1
HΔOv-grn-1
SCR
C
Average indel length (bp)
Mutation type
Adult Deletion
Adult Insertion
NEJ Deletion
Adult flukes
1/13
3/13
11/13
cut
TAATCTCCCAGTGATGA
ORF position (bp)
D
Indel frequency
Individual ΔOv-grn-1 adults
(Indel%)
LΔOv-grn-1 (6 flukes: 0-0.05%)
MΔOv-grn-1 (1 fluke: 3.1%)
HΔOv-grn-1 (6 flukes: 50-91%)
Pooled samples
(Indel%)
SCR NEJ pool
SCR adults pool
ΔOv-grn-1 NEJ pool (3.3%)
-9T
-8C
3G
9T
28A
44C
49T
cut
ORF position (bp)

***Figure 4*. Gene mutation rates among liver flukes**. *Panel **A**, CRISPR/Cas9 gene editing is highly effective in only some flukes. Insertion/deletion (indel) mutation rate ~60 base pairs either side of the CRISPR/Cas9 double stranded break from CRISPResso2 analysis of NGS data, plotted as a violin plot. SCR NEJs and adult flukes are each from a single pooled sample, while ΔOv-grn-1 NEJs are from two biological replicate pooled samples, and ΔOv-grn-1 adult flukes from 13 individual adult flukes. The highly edited flukes are denoted as $_{H}$ΔOv-grn-1, flukes with low editing denoted as $_{L}$ΔOv-grn-1, and flukes with medium level editing denoted as $_{M}$ΔOv-grn-1. One sample t test for either NEJs or adults comparing ΔOv-grn-1 and SCR: * = P<0.05; ** = P<0.01. The thick solid line is the median and the inter-quartiles are black dashed lines. Note the broken Y-axis with a magnified lower portion to highlight the near zero values. **B.** Adult fluke indel mutation rate is inversely correlated with transcript level. The indel and transcript levels plotted for each individual ΔOv-grn-1 fluke (red circles, combining data from Figures 3C and 4A) showed that the highly mutated (>50%, $_{H}$ΔOv-grn-1) flukes generally showed low (<11%) Ov-grn-1 transcript levels, while low edited flukes ($_{L}$ΔOv-grn-1) generally showed higher transcript levels. Highly significant two-tailed non-parametric correlation determined by Spearman co-efficient, r_s = -0.74 (**, P≤ 0.01). The negative linear correlation (slope -0.77) is shown as a red line with shaded 95% confidence intervals (r^2=0.62). For context, the SCR indel% are plotted against the transcript median (blue triangle) with interquartile range error bars. **C.** ΔOv-grn-1 indel location and frequency within adult worms. The NGS sequencing reveals distinct Indel patterns in 12/13 flukes determined with CRISPResso2. Shown as a multivariate bubble plot, the amplicon base pair open reading frame (ORF position) was plotted against the average indel length. The size of the bubbles (1-11) reflects how many of 13 adult flukes recorded a matching indel. The CRISPR/Cas9 cut site between nt 19/20 is marked with "cut". To aid visualization the Adult deletions (blue) and insertions (red) have been nudged up/down on the y-axis +/-0.1. The NEJ deletions (yellow) are shown from one pooled sample and no NEJ insertions were seen. Position -9 is highlighted with a vertical dotted line and the black horizontal square bracket (└─┘) highlights the pre-ORF Indel cluster at positions -1 to -10. The genetic sequence in proximity to this cluster is shown below the x-axis and the ORF initiator methionine sequence (ATG) is highlighted in red. The majority of Indels were 1-4 nt, but a single fluke was recorded with 13 large deletions of 31-62 bp (gray dashed oval). **D.** When successful Ov-grn-1 gene editing was seen, the majority occurred at a single location. The graph plots the Indel position against the frequency with each ΔOv-grn-1 adult Indel shown as individual marks: highly edited ($_{H}$ΔOv-grn-1, green +); medium edited ($_{M}$ΔOv-grn-1, purple +); low edited ($_{L}$ΔOv-grn-1, red x). Pooled samples are shown as ΔOv-grn-1 NEJs (orange circle), SCR NEJs (light blue triangle), and SCR adults (dark blue triangle). A vertical dotted line highlights the hotspot at nt -9 that comprised 98.5-99.9% of the observed indel% for successfully edited ΔOv-grn-1 flukes and NEJs. No $_{L}$ΔOv-grn-1 adults, SCR NEJs or adults showed editing at this position. This hotspot is within the pre-ORF indel cluster at positions -1 to -10 (black horizontal square bracket: └─┘). Other locations with frequently noted indels are labeled with the position number and corresponding nucleotide letter.*

Evaluation of nucleotide position of indels

With respect to indel length and position, mutations were spread 29 bp upstream and 54 bp downstream of the double stranded break (DSB+ (ORF nucleotide position -10 to +74). Most indels were deletions of a single nucleotide, some were as long as four nt and the longest was 62 nt. Deletions were noted along the length of the amplicon, with several higher frequency sites indicated with bubbles of greater diameter in Figure 4C. The pooled NEJ indel locations reflected the high frequency adult locations (Figure 4C, large bubbles). As noted, insertions were infrequently seen but they tended to associate around these high frequency indel locations in NEJs and adult flukes. Of note was the mutation cluster at -1 to -10 bp, within the 5' untranslated region (UTR) of the ORF. Of the 216 indels observed in adult flukes, 48 (22%)

occurred in this region, and five specific sites included indels from 7 or more adult worms. Figure 4D shows the frequency within each sample at each base pair position. Notably, there were hotspot locations in the ORF at which both SCR and Δ*Ov-grn-1* NEJs and adults all showed a mutation, albeit at low frequency. All four ACGT nucleotides were represented in the hotspots. Whereas these hotspots occurred across all groups, they were infrequently seen, with the most common ORF hotspot seen at position 9T in ~0.02% of the genomes sequenced. The 5'UTR cluster at nt position -1 to -10 was also a distinct grouping of mutations in this panel, with no mutations at this location in SCR flukes and only a single $_{L}$Δ*Ov-grn-1* minimally edited fluke in this 10 bp segment. While the cluster was of interest, the striking feature was the highly mutated -9T position. This single position comprised ~99% of the total indel% for $_{M/H}$*ΔOv-grn-1* flukes and *ΔOv-grn-1* NEJs. Despite this single position being highly mutated and the neighboring base pairs comprising the commonly *ΔOv-grn-1* mutated cluster, the next highest frequency position was -8C with only a small proportion of mutated cells recorded (<0.09%).

Programmed knockout of *Ov-grn-1* impeded malignant transformation

The CCA hamster model employed, concurrent liver fluke infection and exposure to DMN [9], induced malignant transformation by the 24 week end point of experiment 2. Predominant lesions of various types were common in all groups, and the high grade CCA whole liver images highlight the most severe pathogenesis from the 24 week infection (Figure 5A, B). Liver pathogenesis such as the pre-cancerous dysplasia stage were evident in many bile duct epithelia and usually surrounded by fibrosis (Figure 5C). Representative micrographs of the high grade cancerous transformation from the three groups are shown in Figure 5D-F. Figure 5G and Table S2 summarize the pathology findings in the three groups of hamsters. Ten of 12 (83.3%) hamsters in the control SCR group were diagnosed with CCA, with high grade CCA in eight of the 10 hamsters and low grade CCA in other two. Dysplasia, a precancerous lesion of CCA [16] was diagnosed in the remaining two of the 12 (one mild, one moderate) hamsters in the SCR group. CCA emerged in seven of 13 hamsters (six with high grade CCA) in the Δ*Ov-tsp-2* group. Of the remaining hamsters, mild dysplasia was seen in two, proliferation in one, inflammation in two, and the final hamster was free of hepatobiliary lesions. CAA was diagnosed in nine of 13 in the *ΔOv-grn-1* group, four with high grade CCA. Of the remaining hamsters, one showed moderate dysplasia, two showed proliferation, and one was free of apparent hepatobiliary lesions. Lesions less severe than dysplasia, i.e. inflammation, proliferation, or no lesions, were evident in several hamsters infected with Δ*Ov-tsp-2* (4/13 hamsters) and Δ*Ov-grn-1* flukes (3/13 hamsters).

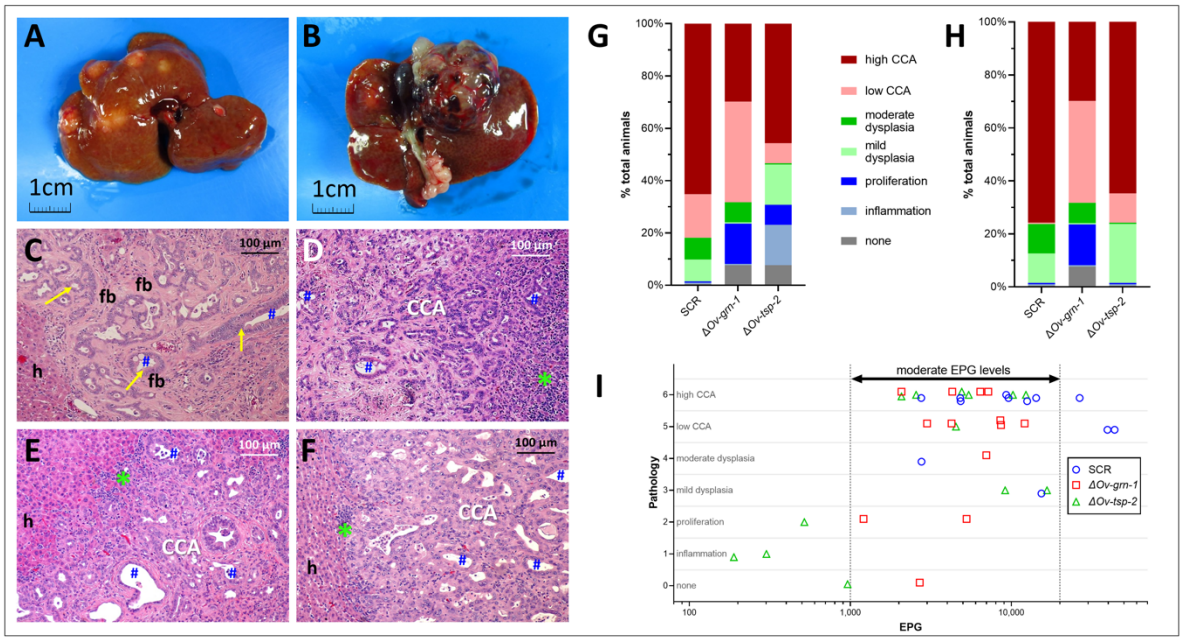

Figure 5. Hepatobiliary disease burden in liver fluke infection associated cholangiocarcinoma. *Livers were harvested and a component of each lobe was prepared for sectioning or used for harvesting flukes for subsequent analysis (Fig. 1, Experiment 2). Gross appearance and histopathological results from cholangiocarcinoma [1] induction using dimethyl nitrosamine (DMN) and gene edited newly excysted juveniles (NEJ) infection. Multiple CCA nodules in the hamster liver presented in both diaphragmatic* ***(A)*** *and visceral surfaces* ***(B)****. H&E stained histology slide highlighting foci of moderate dysplasia* ***(C).*** *This image consists of bile ducts (blue #) encircled by dysplastic biliary epithelium (yellow arrow) surrounded by fibrosis (fb) with hepatocytes (h) to the left. Histological H&E stained images of CCA from each of the hamster groups: SCR* ***(D),*** *ΔOv-grn-1* ***(E),*** *and ΔOv-tsp-2* ***(F)****. Inflammation marked with (green asterisk *), cholangiocarcinoma labelled with CCA and other labels are as detailed in panel C. Euthanized hamster livers were sectioned and examined for degree of pathogenesis.* ***G.*** *Assessment of the highest degree of pathological lesions or CCA development present in entire liver sections of all animals was conducted by two experienced veterinary pathologists using blinded H&E stained slides. The lesions increased in severity from none (grey) to high grade CCA (red) spanning multiple liver lobes.* ***H****. The gross overall liver pathology with only "moderate EPG" phenotype hamsters. If no animal was noted in a category, a thin band of color is shown.* ***I.*** *EPG from individual hamsters plotted against the pathology status on a scale of zero (0, no lesion) to 6 (high CCA) scale. The cutoffs for 1,000 to 20,000 "moderate EPG" data are highlighted with vertical dashed lines. Data points were nudged ± 0.1 on the Y-axis to mitigate e the display of overlapping points. Hamsters with EPG >1,000 did not show significant correlation between EPG and pathogenesis (two-tailed non-parametric Spearman correlation, P>0.05).*

There was no substantial difference in the location or subtype of CCA tumors among the treatment groups. The CCA tumors observed ranged in sizes from small neoplasms with multifocal distributions (10/24) to fully developed tumor masses visible to the unaided eye (14/24) (Figure 5). With respect to histological classification, 19 of 24 were of the tubular type [2]. One papillary/cystic CCA was seen in the *ΔOv-grn-1* group and as was the mucinous type CCA in one SCR- and three *ΔOv-tsp-2 O. viverrini*-infected hamsters. The right lobe was the

365 frequent location of the tumor in all hamsters (20/26), with nine in the left lobe, and three in the
366 middle lobe. Occasionally, tumors had developed in more than one lobe (5/26) but usually
367 occurred in a single lobe (21/26).
368
369 The pattern of pathogenesis in "moderate EPG" animals was similar to that for the SCR animals,
370 showing dysplasia to CCA, with the most common pathogenesis of CCA in 78% of animals, and
371 100% of these were high grade (Figure 5H). No animals were excluded from the *ΔOv-grn-1*
372 group and the 69% CCA rate was retained, of which 44% were high grade CCA. The *ΔOv-tsp-2*
373 group changed substantially and resembled the SCR group when only "moderate EPG" animals
374 were included. As with the SCR group hamsters, dysplasia was the minimum pathological lesion
375 and 78% had CCA, with most (86%) being high grade CCA. We assessed pathology in relation
376 to EPG levels (Figure 5, panel I) and noted that low pathogenesis was observed in *ΔOv-tsp-2*
377 hamsters with low EPG (<1,000). Beyond the arbitrary threshold of 1,000 EPG, |no correlation
378 was apparent with level of pathology; the two SCR animals with the highest EPG recorded low
379 grade CCA and degrees of dysplasia seen across the EPG range. Although we posit that at
380 euthanasia 24 weeks after infection *ΔOv-tsp-2* group hamsters were infected with fewer adult
381 stage liver flukes than the other groups, the similar pattern in hepatobiliary tract lesions in both
382 the SCR and *ΔOv-tsp-2* groups with the moderate EPG phenotype indicated that the damage
383 caused by chronic opisthorchiasis was similar, at and beyond a threshold number of parasites.
384 Subsequently, we focused assessments of histopathology only on the hamsters with the
385 "moderate EPG" phenotype.
386
387 **Reduced biliary tract fibrosis during infection with knockout parasites**
388
389 Hepatic fibrosis was detected in Picro-Sirius Red (PSR)-stained thin tissue sections and enabled
390 investigation and quantification of peribiliary fibrotic development (Figure 6A), using an
391 automated, visual quantitation. Fibrosis was evaluated, firstly on Ishak stage, a semi-quantitative
392 measure of the degree of fibrosis spread across the liver parenchyma [17], and secondly, on the
393 fibrotic deposition localized around the liver flukes, i.e. the amount of collagen deposition
394 surrounding bile ducts occupied by parasites at the time of necropsy.
395
396 The Ishak scores correspond to degrees of damaging liver fibrosis and the levels reflect fibrotic
397 expansion in periportal areas and the degree of bridging between portal regions, increasing up to
398 level 6 with full cirrhosis (Figure 6B). The control (SCR) group was the most severely affected,
399 with the livers of all hamsters assigned an Ishak score of 4. This indicated that fibrosis had
400 progressed extensively with marked portal-portal and portal-central bridging. Hamsters in the
401 *ΔOv-grn-1* group showed a median Ishak grade of 2 (range 2 to 4), with fibrosis in most portal
402 areas with/without short fibrous septa that had not bridged to other portal regions. Hamsters
403 infected with the *ΔOv-tsp-2* liver flukes showed a median Ishak score of 3 (range 2 to 4). This is
404 defined as fibrous expansion of most portal areas with occasional bridging between them [17].
405 The *ΔOv-tsp-2* group was not significantly different to the control group, whereas the *ΔOv-grn-1*
406 group had significantly less fibrosis compared to either SCR ($P \leq 0.0001$) or *ΔOv-tsp-2* ($P \leq 0.05$)
407 groups.
408
409
410

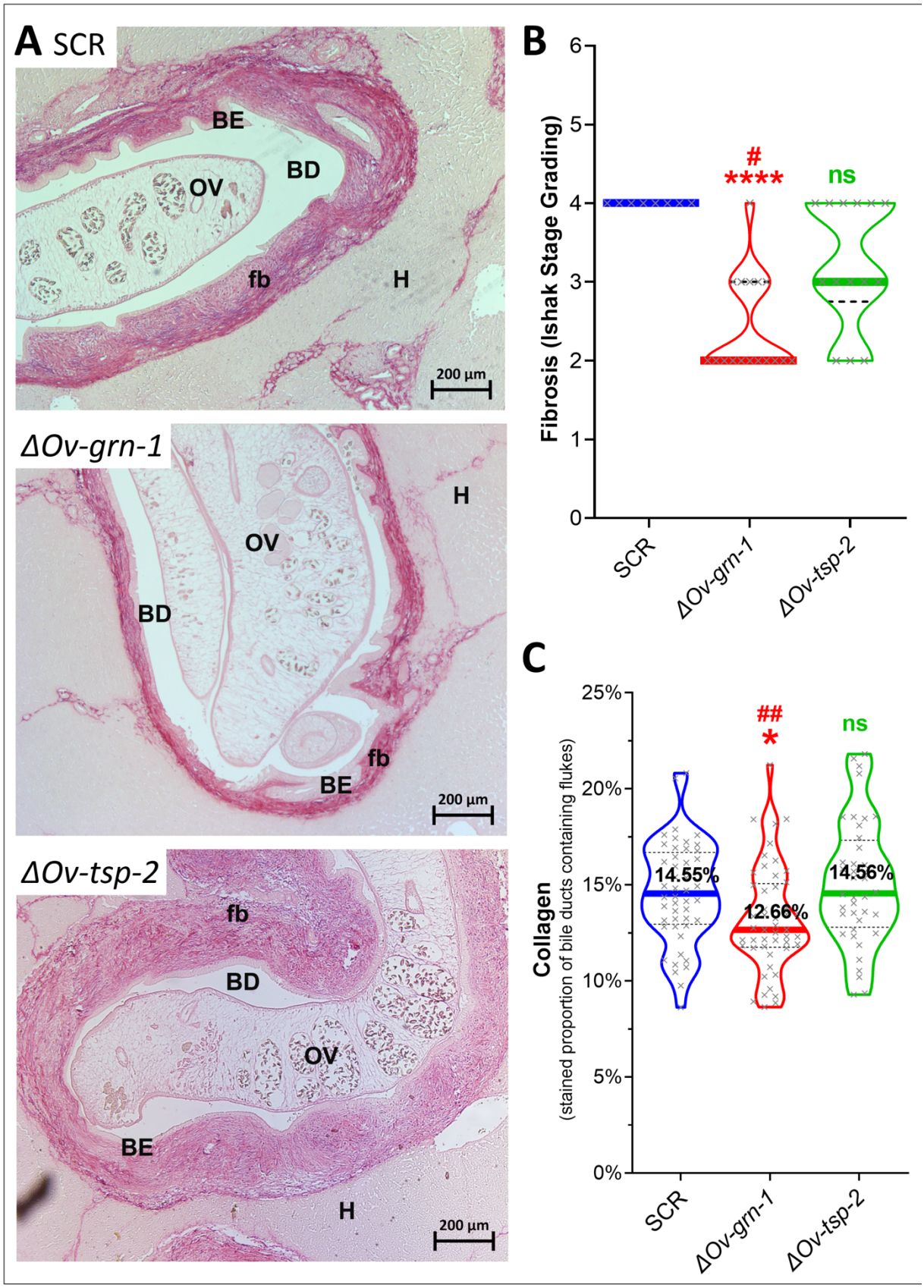
A SCR
BE
BD
OV
fb
H
200 µm
ΔOv-grn-1
H
OV
BD
fb
BE
200 µm
ΔOv-tsp-2
fb
BD
OV
BE
H
200 µm
B
Fibrosis (Ishak Stage Grading)
0
1
2
3
4
5
6
#
****
ns
SCR
ΔOv-grn-1
ΔOv-tsp-2
C
Collagen
(stained proportion of bile ducts containing flukes)
0%
5%
10%
15%
20%
25%
##
*
ns
14.55%
12.66%
14.56%
SCR
ΔOv-grn-1
ΔOv-tsp-2

***Figure 6**. **Attenuated hepatic fibrosis during infection with ΔOv-grn-1 gene edited liver flukes**. **A.** Representative images of hepatic fibrosis stained by Picro-Sirius Red with CRISPR-Cas9 edited O . viverrini from the 24-week CCA model. Fibrosis is denoted as pink/red thick bands around the bile ducts (periductal fibrosis, fb) and expands from each portal triad with fibrous septa. OV = Opisthorchis viverrini fluke, H = hepatocytes, BD = bile duct, BE = biliary epithelium. **B**. Global liver fibrosis plotted as a violin plot. Livers were scored for pathogenic fibrosis with an Ishak Stage Grading scale and plotted on a violin graph that spans from zero (no fibrosis) to six (cirrhosis). **C.** Fibrosis proximal to flukes plotted as a violin plot. Automated ImageJ fibrosis analyzer software evaluation of the percentage of collagen deposition in images surrounding fluke-containing bile ducts. Panels B+C: median shown as thick colored line and dashed black lines mark the inter-quartile ranges. Comparing groups with Kruskal-Wallis test with Dunn's multiple comparisons against SCR: ns = not significant; **, $P \leq 0.05$; ***, $P \leq 0.0001$, and against ΔOv-tsp-2 group: #, $P \leq 0.05$; ##, $P \leq 0.01$.*

To assess localized fibrosis specifically in the area where flukes were detected, we investigated the degree of periductal fibrosis immediately proximal to live flukes in the bile duct lumen. Automated analysis of the collagen deposition surrounding the bile ducts was undertaken using an ImageJ driven fibrosis quantification tool of the PSR-stained collagen. Of the bile duct tissue surrounding SCR and *ΔOv-tsp-2* flukes, 14.55% and 14.56% of the tissue was fibrotic, whereas 12.66% of bile duct tissue surrounding *ΔOv-grn-1* flukes was fibrotic (Figure 6C, $P \leq 0.05$).

Ov-grn-1 gene edited flukes drive less cell proliferation than control flukes

Here, we explored the *in vivo* effects as a consequence of programmed knockout of *Ov-grn-1* expression, following our earlier reports which centered on proliferation of the biliary epithelium and/or cultured cholangiocytes in response to *in vitro* exposure to *Ov*-GRN-1 [5, 18-21]. Proliferation of hamster biliary cells *in situ* was investigated using BrdU where the thymine analogue BrdU is incorporated into cellular DNA. Visualization was performed using immunohistochemistry (Figure 7A) and evaluated quantitatively. Concerning worm survival, and its corollary, the fitness cost of the programmed mutation, we examined proliferation but only in the bile ducts where flukes were situated. Median proliferation in bile duct tissue surrounding liver flukes in the SCR (15.0%) and *ΔOv-tsp-2* (11.1%) groups were not significantly different from each other, whereas only 3.1% of bile duct tissue surrounding *ΔOv-grn-1* flukes had incorporated BrdU ($P<0.0001$ vs SCR; $P<0.05$ vs *ΔOv-tsp-2*, Figure 7B). By contrast, the *ΔOv-grn-1* group (3.1%) showed significantly less proliferation than both the SCR, 4.8-fold reduction ($P<0.0001$) and the *ΔOv-tsp-2* group, 3.6-fold reduction ($P<0.05$).

Mutant _TP53_ less frequent during infection with _Ov-grn-1_ gene edited flukes

Tumor protein p53 plays a well-recognized role in cholangiocarcinogenesis and is highly expressed in fluke infection associated CCA cells [2, 22]. Brown nuclear staining pattern presents only in neoplastic biliary cells (Figure 7C). Wide angle images of flukes in the biliary tract showed mutant p53 positive and negative cells in the epithelium. The p53 staining was significantly different among the groups: SCR and *ΔOv-tsp-2* fluke infected hamsters showed 61.1 and 67.5% of cholangiocytes staining positive for p53 (not significant), respectively, whereas only 7.5% of cholangiocytes were positive in *ΔOv-grn-1* infected animals (~9-fold reduction, $P<0.01$) (Figure 7D).

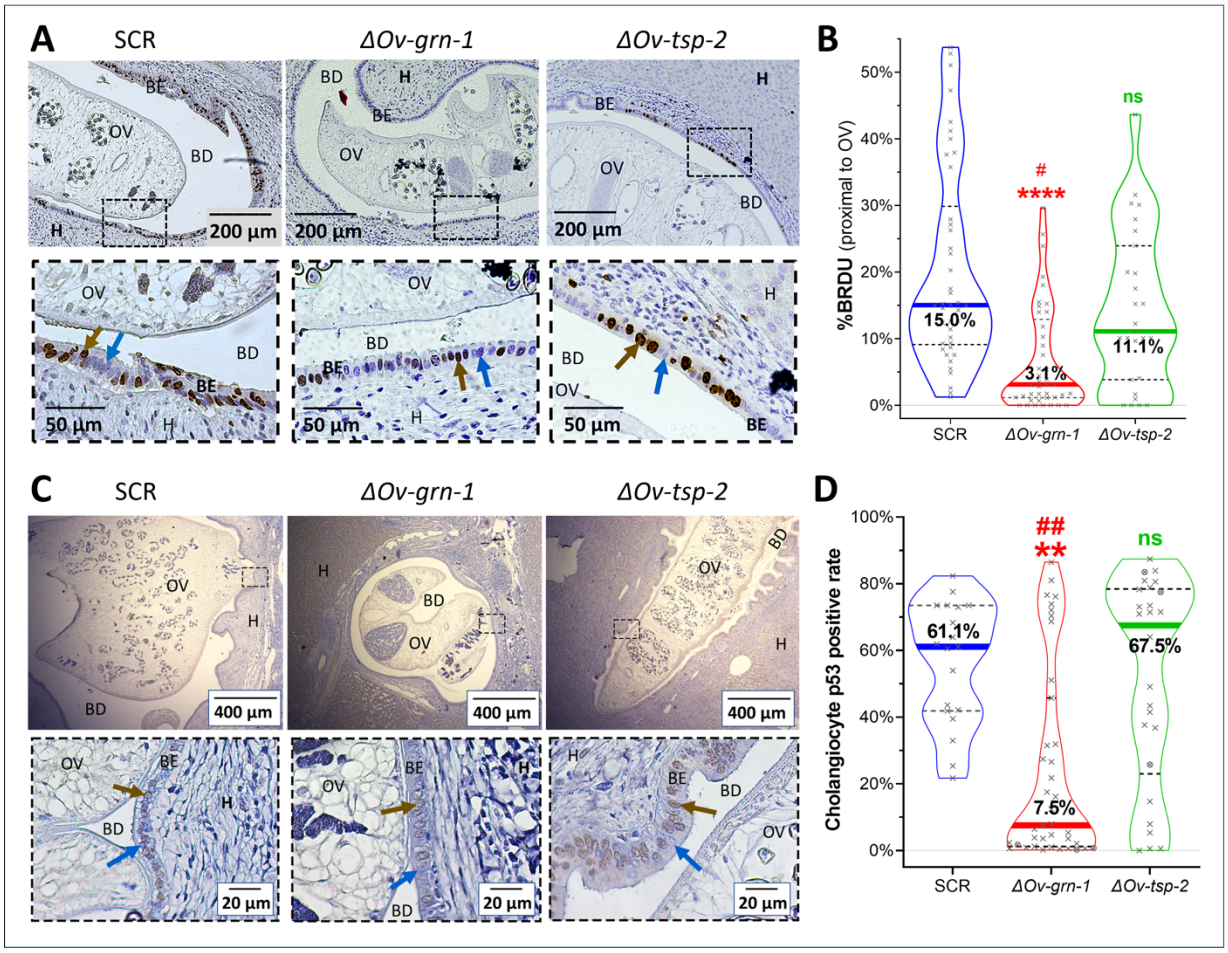

446

Figure 7. Reduced cholangiocyte proliferation and p53 expression during infection with ΔOv-grn-1 genotype liver flukes. *Representative images of proliferating biliary cells that incorporated BrdU from liver samples proximal to flukes in SCR, ΔOv-grn-1 and ΔOv-tsp-2 groups* ***(A)****. The boxed region in the upper image is magnified in the lower panel. The brown arrow highlights the positive BrdU-stained nuclei in each image and the blue arrow highlights a negative bile duct cell that did not incorporate BrdU. Violin graphs of BrdU index measured from cholangiocytes in bile ducts containing a fluke* ***(B)****. Representative micrograph of p53 immunohistochemistry of biliary epithelium of DMN-exposed hamsters infected with gene edited liver flukes* ***(C).*** *Anti-p53 antibody stained nuclei brown (brown arrows); unstained negative cells indicated using blue arrows. Black dashed box in upper wide-angle image is magnified in the lower image to aid visualization. Violin plot of p53 positive cholangiocytes as a percentage* ***(D).*** *Where available, 500 to 800 cells were scored from sections of each of the left, middle, and right lobes of the liver of hamsters with "moderate EPG", and marked by a grey "x". In a few samples, three ΔOv-grn-1 lobes and three ΔOv-tsp-2 lobes, only 300-500 cholangiocytes were available for assessment of p53 status; here, all the cholangiocytes were counted and marked with ⓧ. Panels A+C: OV = Opisthorchis viverrini fluke, H = hepatocytes, BD = bile duct, BE = biliary epithelium. Panels B, D: non-parametric Kruskal-Wallis test with Dunn's multiple comparison correction compared against SCR: ns = not significant; **, P≤ 0.01; ****, P ≤ 0.0001, or against ΔOv-tsp-2: ns, not significant; #, P ≤ 0.05; #, P≤0.01. Thick colored lines signify the median and the dashed black lines mark the inter-quartile ranges.*

447 **Discussion**
448
449 Cholangiocarcinoma (CCA) accounts for ~15% of all primary liver cancers and its incidence
450 rates are increasing [23]. Infection with the foodborne liver fluke, *Opisthorchis viverrini*, is the
451 principal risk factor for CCA in the Lower Mekong River Basin countries including Thailand and
452 Laos PDR [2, 11, 24]. In an earlier report, we exploited this link to explore the role of a growth
453 factor, liver fluke granulin, Ov-GRN-1, secreted by the parasite in tumorigenesis using
454 programmed gene knockout, and reported that the infection was less severe although gene-edited
455 parasites colonized the biliary tract of hamsters and developed into adult flukes [7].
456
457 Here, we utilized an established model of opisthorchiasis-associated CCA in hamsters that were
458 infected with the parasite during concurrent exposure to exogenous nitrosamine. CCA manifests
459 under these conditions, and this rodent model reflects the human situation where chronic
460 opisthorchiasis combined with a diet that is rich in fermented fish (in turn, rich in exogenous
461 nitrosamines) culminates in high incidence of CCA [10, 11, 25, 26]. In hamsters, opisthorchiasis
462 leads to periductal fibrosis. Severe periductal fibrosis combined with a nitric oxide carcinogen,
463 such as DMN, results in epithelial cholangiocyte proliferation, hyperplasia, dysplasia, and DNA
464 damage, eventually culminating in malignant transformation of the biliary tract [10, 27]. The
465 current findings confirmed a role for *Ov*-GRN-1 in opisthorchiasis-associated malignancy.
466 Markedly less proliferation of the biliary epithelium, mutant p53 expression in cholangiocytes,
467 and periductal fibrosis were observed during infection with *ΔOv-grn-1* worms. Furthermore, we
468 report a functional genomics approach-based expansion of the model pioneered more than 30
469 years ago [9], which involved concurrent administration of nitrosamine during infection with
470 gene-edited *O. viverrini*.
471
472 The fitness cost of gene knockout can be assessed from programmed gene editing, an approach
473 that is employed for the unbiased identification of essential genes in other organisms and disease
474 settings [28, 29]. Our present findings confirmed the power of RNA-guided targeted mutation to
475 define essentiality and relevance of parasite proteins in infection-associated morbidity and
476 malignancy. The *Ov-grn-1* gene does not appear to essential for *in vivo* development and
477 survival, which has enabled investigation here on the role of this protein in driving cell
478 proliferation, pathology and ultimately contributing to CCA *in vivo*. Nonetheless, the reduced
479 fecundity of *ΔOv-grn-1* liver flukes likely reflected a fitness deficit as the result of targeted gene
480 knockout. By contrast, *Ov-tsp-2* appears to be essential to parasitism, since the *ΔOv-tsp-2*
481 genotype did not survive, and sequencing of the indels across the relevant region of the genome
482 confirmed that most of the surviving flukes from hamsters had undergone minimal or no editing
483 of the *Ov-tsp-2* gene. These findings build upon earlier RNA interference-mediated silencing of
484 *Ov-tsp-2* gene expression and the corresponding malformation of the tegument observed *in vitro*
485 [30]. Although *Ov-tsp-2* dsRNA-treated parasites were not used for *in vivo* studies, the damage
486 to the tegument was extensive and survival *in vivo* of worms damaged to that extent appeared to
487 be unlikely.
488
489 Although the primary goal of this investigation was to characterize pathogenesis and pathology
490 associated with infection with *ΔOv-grn-1* flukes, and infection in the absence of Ov-GRN-1, we
491 investigated the mutation profile induced by our gene-editing system. Intriguingly, most
492 mutations in the *Ov-grn-1* targeted gene editing took place in the 5'UTR, and the majority

493 (~99%) of the mutations centered on a single position (-9T) position, 28 bp 5' to the
494 programmed CRISPR/Cas9 double strand break (DSB) at nucleotide positions 19 and 20 of the
495 ORF. This was unpredicted given that mutations were expected at the programmed DSB [7]. The
496 sequence of the 5'UTR of *Ov-grn-1* does not exhibit identity to regulatory elements in the UTR
497 database, http://utrdb.ba.itb.cnr.it/, perhaps not unexpectedly given that few helminth parasite
498 UTR regulatory elements have been characterized [31]. Why this position was preferentially
499 mutated is unclear; however, the marked reduction of transcription of *Ov-grn-1* that
500 accompanied this mutation profile, which was localized in the 5'UTR, suggests the presence of
501 an active regulatory control element.
502
503 Chronic liver fibrosis is a risk factor for liver cancer. The traditional lifestyle of people living in
504 *O. viverrini*-endemic areas, notably a diet enriched in nitrosamines as well as routine use of
505 alcohol, when coupled with the assault on the biliary epithelium by the attachment, feeding,
506 movement, and secretions of the liver flukes that result in repeated cycles of injury and repair
507 cycles, establishes a compelling setting for malignant transformation [32-34]. The secretion of
508 liver fluke granulin into the bile ducts and its ability to relentlessly drive cell proliferation and to
509 (re)heal wounds inflicted by the parasite plays a central role in this process [19]. Knockout
510 mutation of *Ov-grn-1* did not substantially thwart infection, development and survival of the
511 liver fluke *in vivo* but infection with these *ΔOv-grn-1* flukes failed to lead to the marked cell
512 proliferation and fibrosis in the immediate vicinity of the parasites, and consequently fewer
513 hamsters developed with high-grade CCA compared with the infections with the control SCR
514 and *ΔOv-tsp-2* parasites. Indeed, more hamsters infected with *ΔOv-grn-1* flukes were diagnosed
515 in the low-CCA and the proliferation categories than in the other treatment groups. Knockout
516 mutation of *Ov-grn-1* attenuated virulence and impeded malignant transformation during chronic
517 opisthorchiasis.
518
519 Infected hamsters exhibited elevated rates of *TP53* mutation although the level was markedly
520 less during infection with *ΔOv-grn-1* flukes. The mutational signatures and related molecular
521 pathways characteristic of human CCAs have been reviewed in depth, and the signature profiles
522 differ between fluke associated and non-fluke associated CCAs [2]. Fluke associated CCAs
523 exhibit substantially more somatic mutations than non-fluke related CCAs [22], likely the
524 consequence of opisthorchiasis-associated chronic inflammation. In conformity with the human
525 situation, reduced inflammation and fibrosis were seen in hamsters infected with the *ΔOv-grn-1*
526 flukes, further emphasizing the virulence of this growth factor in chronic opisthorchiasis.
527 Inactivating mutations of *TP53* are more prevalent in this subgroup, as are mutations of *ARID1A,*
528 *ARID2*, *BRCA1* and *BRCA2*, than in non-fluke related CCAs [22, 35-38]. In addition,
529 hypermethylation has been noted for the promoter CpG islands of several other aberrantly
530 expressed genes [22].
531
532 Mosaicism of gene knock-out is a limitation of our somatic gene-editing approach. Obviating
533 mosaicism by derivation of transgenic worms following germ line transgenesis is unlikely in the
534 near future in the context of this multicellular eukaryote, especially when overlaid on the genetic
535 complexity of a hermaphroditic platyhelminth parasite with a diploid genome. In addition, this
536 parasite has a multiple host developmental cycle, which cannot reliably be reproduced in the
537 laboratory. Nonetheless, somatic genome editing is of increasing utility in biomedicine,
538 including for treatment of hemoglobinopathies [39] and in the identification of targets for disease

539 interventions [40]. Given the role of *Ov*-GRN-1 as a virulence factor in opisthorchiasis,
540 interventions that target this growth factor might be beneficial. Indeed, antibodies raised against
541 recombinant *Ov*-GRN-1 block its ability to drive proliferation of CCA cell lines [5], and
542 vaccination strategies that target *Ov*-GRN-1 in the GI tract, for example through induction of
543 mucosal IgA and IgG responses [41, 42] should be explored, and might form a valuable
544 component of a multivalent, orally administered, anti-infection and anti-cancer vaccine [2, 42].
545
546 **Materials and methods**
547
548 **Metacercariae, newly excysted juvenile and adult developmental stages of *O .viverrini***
549
550 Metacercariae (MC) of *O .viverrini* were obtained from naturally infected cyprinid fish
551 purchased from local food markets in the northeastern provinces of Thailand. MC were isolated
552 from fishes by using pepsin digestion as described previously [43]. Briefly, whole fishes were
553 minced by electric blender and digested with 0.25% pepsin with 1.5% HCl in 0.85% NaCl at 37
554 ºC for 120 min. The digested fishes were filtered sequentially through sieves of 1,100, 350, 250,
555 and 140 µm mesh apertures. The filtered digest of fish flesh was subjected to gravity
556 sedimentation in a sediment jar through several changes of 0.85% NaCl until the supernatant was
557 clear. MC in the sediment were identified under a dissecting microscope as *O. viverrini* and
558 active (larval movement within the cyst) *O. viverrini* MC were stored in 0.85% NaCl at 4ºC until
559 used.
560
561 Newly excysted juveniles of *O. viverrini* (NEJ) were induced to escape from the metacercarial
562 cyst by incubation in 0.25% trypsin in PBS supplemented with 2× 200 U/ml penicillin, 200
563 µg/ml streptomycin (2× Pen/Strep) for 5 min at 37°C in 5% CO_2 in air. NEJ were isolated free of
564 discarded cyst walls by mechanical passage through a 22 G needle [7] .
565
566 **Plasmid constructs and transfection of *O. viverrini* NEJ**
567
568 The CRISPR plasmid encoding a guide RNA (gRNA) complimentary to *Ov-grn-1* exon 1 termed
569 pCas-*Ov-grn-1* was constructed using the GeneArt CRISPR Nuclease Vector kit (Thermo Fisher
570 Scientific) as described [7]. The programmed cleavage site at nucleotide position 1589–1608, 5'-
571 GATTCATCTACAAGTGTTGA with a CGG proto-spacer adjacent motif (PAM) which
572 determined the cleavage site located at three nucleotides upstream on *Ov-grn-1* was designed
573 using the online tools, http://crispr.mit.edu/ [44] and
574 CHOPCHOP, http://chopchop.cbu.uib.no/ [45, 46] using the *Ov-grn-1* gene (6,287 bp,
575 GenBank FJ436341.1) as the reference. A second plasmid, termed pCas-*Ov-tsp-2* was
576 constructed using the same approach; pCas-*Ov-tsp-2* encodes a gRNA targeting exon 5 of the
577 *Ov-tsp-2* gene (10,424 bp, GenBank JQ678707.1) [47, 48]. The guide RNAs encoded by *Ov-grn-*
578 *1* and *Ov-tsp-2* exhibited high on-target efficiency and little or no off-target matches to the *O.*
579 *viverrini* genome. A third construct termed pCas-*Ov*-scramble was also prepared and included as
580 a control to normalize analysis of gene expression and programmed gene knockout. The pCas-
581 *Ov*-scramble construct included as the gRNA, a transcript of 20 nt, 5'-
582 GCACTACCAGAGCTAACTCA which exhibits only minimal identity to the *O. viverrini*
583 genome and which lack a PAM [49]. A mammalian U6 promoter drives transcription of the
584 gRNAs in all three plasmids and the CMV promoter drives expression of the *Streptococcus*

585 *pyogenes* Cas9 nuclease (modified to include the eukaryotic nuclear localization signals 1 and 2).
586 To confirm the orientation and sequences of gRNA in the plasmid vector, *Escherichia coli*
587 competent cells (TOP10) were transformed with the plasmids, plasmid DNAs were recovered
588 from ampicillin resistant colonies using a kit (NucleoBond Xtra Midi, Macherey-Nagel GmbH,
589 Düren, Germany), and the nucleotide sequences of each construct confirmed as correct by
590 Sanger direct cycle sequencing using a U6-specific sequencing primer.
591
592 Two hundred NEJs of *O. viverrini* were dispensed into an electroporation cuvette, 4 mm gap
593 (Bio-Rad, Hercules, CA) containing 20 µg pCas-*Ov-grn-1,* pCas-*Ov-tsp-2* or pCas-*Ov*-scramble
594 in a total volume of 500 µl RPMI, and subjected to a single square wave pulse at 125 V for 20
595 ms (Gene Pulser Xcell, Bio-Rad). The NEJ were cultured in RPMI supplemented to 1% glucose
596 for 60 min after which they were used for infection of hamsters by stomach gavage (below).
597
598 **Infection of hamsters with gene edited NEJs**
599
600 Figure 1 provides a timeline of the CCA model, employed in experiment 1 and 2. In a first
601 experiment, nine male hamsters aged between 6-8 weeks were randomly divided into three
602 experimental groups (Figure 1). Each hamster was infected with 100 *O. viverrini* NEJs. These
603 NEJs had been transfected with pCas-*Ov-grn-1* plasmid, pCas-*Ov-tsp-2*, or the control pCas-*Ov*-
604 scramble, and assigned the following identifiers: delta(Δ)-*gene* name, Δ*Ov-grn-1, ΔOv-tsp-2,* or
605 SCR, respectively. These NEJs had been transfected with pCas-*Ov-grn-1* plasmid, pCas-*Ov-tsp-*
606 *2*, or the control pCas-*Ov*-scramble, and assigned the following identifiers: delta(Δ)-*gene* name,
607 Δ*Ov-grn-1, ΔOv-tsp-2,* or SCR, respectively. The hamsters were infected with NEJ by gastric
608 gavage The infected hamsters were maintained under a standard light cycle (12 hours dark/light)
609 with access to water and food *ad libitum*. At day 14 following infection, the water accessed by
610 the hamsters was replaced with drinking water supplemented with dimethylnitrosamine (DMN)
611 (synonym, *N*-nitrosodimethylamine) (Sigma-Aldrich, Inc., St. Louis, MO) at 12.5 ppm, which
612 was maintained until 10 weeks following infection [8-10]. Hamster feces were collected at weeks
613 10 and 12 after infection for fecal egg counts. The hamsters were euthanized at week 14 after
614 infection via isoflurane inhalation, livers were collected, and numbers of liver flukes counted.
615
616 In the second experiment, 45 male Syrian golden hamsters, *Mesocricetus auratus*, 6–8 weeks of
617 age, were randomly divided into three groups each with 15 hamsters and infected with gene
618 edited NEJs (above). These NEJs had been transfected with pCas-*Ov-grn-1* plasmid, pCas-*Ov-*
619 *tsp-2*, or the control pCas-*Ov*-scramble, and assigned the following identifiers: delta(Δ)-*gene*
620 name, Δ*Ov-grn-1, ΔOv-tsp-2,* or SCR, respectively. The NEJ were introduced into the hamster
621 stomach using an orogastric tube. The infected hamsters were maintained under a standard light
622 cycle (12 hours dark/light) with access to water and food *ad libitum*. At day 14 following
623 infection, the water accessed by the hamsters was replaced with drinking water supplemented
624 with DMN at 12.5 ppm, which was maintained until 10 weeks following infection, as above.
625 Hamster feces were collected at week 23 after infection for fecal egg counts. At week 24, 40
626 mg/kg thymine analogue 5-bromo-2'-deoxyuridine (BrdU, Abcam, College Science Park, UK)
627 was introduced into the peritoneum of the hamsters at 30 min before euthanasia,, to incorporate
628 the thymidine analogue into the nuclei to enable investigation of proliferation of the biliary
629 epithelia post-mortem [50]. Hamsters were euthanized, the liver resected from each hamster at
630 necropsy, the liver lobes separated, and the left, middle and right lobes fixed in 10% formalin.

631 We have used the shorthand to identify the lobes; left (left dorsocaudal), middle (combined
632 ventral and dorsal median lobes), and right (right dorsocaudal). Liver flukes recovered from the
633 hepatobiliary tract were stored in RNAlater (Thermo Fisher) for subsequent analysis of gene
634 expression, gene-editing efficiency, and indel profile.
635
636 All the hamsters were maintained at the animal rearing facility of the Faculty of Medicine, Khon
637 Kaen University, Khon Kaen. The protocol was approved by the Animal Ethics Committee of
638 Khon Kaen University, approval number ACUC-KKU-61/60, which adhered to the guidelines
639 prescribed by the National Research Council of Thailand for the Ethics of Animal
640 Experimentation.
641
642 **Histopathological investigation of hepatobiliary tissues**
643
644 Whole hamster livers were dissected and fixed in 10% buffered formalin. After overnight
645 fixation, specimens were further routinely processed for paraffin embedding by dehydration in a
646 series of 70%, 90%, and 100% ethanol, cleared in xylene and infiltrated in melted paraffin before
647 being embedded in paraffin block. Four µm liver sections were obtained using a microtome and
648 stained with hematoxylin and eosin (H&E) for histopathologic evaluation of the hepatobiliary
649 system. Histopathological grading criteria of the liver and bile duct of hamsters was scored for
650 the extent of bile duct inflammation, bile duct changes, dysplasia (including dysplasia in
651 cholangiofibrosis) and stage of CCA as described [27, 51-53], with modifications (Table 1).
652
653 **Table 1**. Criteria for histopathological and histochemical assessment
654

Histopathological lesion	Grade description	Reference
Inflammation	0 = None (no/minimal liver tissue or portal inflammation) 1 = Mild (1-2 foci per 4× objective at hepatocyte & periportal area) 2 = Moderate (3-5 foci per 4× objective at hepatocyte & periportal area) 3 = Severe (> 5 foci per 4× objective at hepatocyte & periportal area)	[27, 53, 54]
Bile duct changes	0 = None (absent proliferation and cholangiofibrosis) 1 = Mild (bile duct proliferation without cholangiofibrosis or periductal fibrosis) 2 = Moderate (bile duct proliferation with cholangiofibrosis) 3 = Severe (bile duct proliferation with cholangiofibrosis and periductal fibrosis)	[27, 53, 54]
Dysplasia	0 = None (No cellular atypia, no nuclear polarity, no protruding of nuclei, no nuclear pseudostratification) 1 = Mild (Cellular atypia+, no nuclear polarity, no protruding of nuclei, nuclear pseudostratification+, nuclei within the lower two-thirds) 2 = Moderate (Cellular atypia+, nuclear polarity+, protruding of nuclei+, nuclear pseudostratification+) 3 = High (Cellular atypia++, nuclear polarity++, protruding of nuclei+, nuclear pseudostratification+)	[52]

Cholangiocarcinoma	0 = None (no evident of CCA) Low CCA: 1 = Mild (CCA area 1-2 foci per 4× objective) High CCA: combined 2+3: 2 = Moderate (CCA area 3-5 foci per 4× objective) and 3 = Severe (CCA area> 5 foci per 4× objective)	[27, 53, 54]
Fibrosis (PSR stain): Ishak score	0 =No fibrosis 1 = Fibrous expansion of some portal areas, with or without short fibrous septa 2 = Fibrous expansion of most portal areas, with or without short fibrous septa 3 = Fibrous expansion of most portal areas with occasional portal to portal bridging 4 = Fibrous expansion of portal areas with marked bridging (portal to portal as well as portal to central) 5 = Marked bridging (portal–portal and/or portal–central) with occasional nodules (incomplete cirrhosis) 6 = Cirrhosis, probable or definite	[55] [17]
Assessment of collagen proximal to liver flukes	Quantitative automated evaluation of collagen deposition percentage surrounding bile ducts	ImageJ software "MRI Fibrosis quantification tool" macro (Volker Bäcker 2015, (INSERM; Montpellier RIO Imaging, www.mri.cnrs.fr

655
656 **Fecal egg counts and worm counts**
657
658 Feces from each hamster was individually collected, weighed and *O. viverrini* eggs per gram of
659 feces (EPG) calculated using a modified formalin-ethyl acetate technique [56]. In brief, hamster
660 feces were collected and fixed in 10 ml of 10% formalin. Thereafter, the slurry of formalin-fixed
661 feces was filtered through two layers of gauze, and clarified by centrifugation at 500 *g* for 2 min.
662 The pellet was resuspended with 7 ml of 10% formalin, mixed with 3 ml ethyl-acetate and
663 pelleted at 500 *g* for 5 min. The pellet was resuspended in 10% formalin solution and examined
664 at 400× by light microscopy. EPG was calculated as follows: (average number eggs × total drops
665 of fecal solution)/ gram of feces. To recover the adult liver flukes, food was withdrawn from the
666 hamsters 16 hours before euthanasia. At necropsy, terminal blood was collected from the heart
667 and allowed to clot at 4˚C for 30 min followed by centrifugation at 2,100 *g* for 10 min. The
668 clotted-blood serum was stored at -20˚C. Intact mature *O. viverrini* from the hepatobiliary tract
669 were recovered during observation of the livers using a stereo dissecting microscope and stored
670 for downstream gene-editing investigation.
671
672 **Extraction of nucleic acids**
673
674 Pooled NEJ or single mature worms from either experimental or control groups were
675 homogenized in RNAzol RT (Molecular Research Center, Inc., Cincinnati, OH) before dual
676 RNA and DNA extraction as described [7]. Briefly, the parasite(s) were homogenized in

677 RNAzol RT using a motorized pestle, after which the DNA and protein were precipitated in
678 nuclease free water. The aqueous upper phase was transferred into a new tube for total RNA
679 precipitation by isopropanol (50% v/v). The DNA/protein pellet was resuspended in DNAzol and
680 genomic DNA extracted according to the manufacturer's instructions (Molecular Research
681 Center). Concentration and integrity of genomic DNA and total RNA were independently
682 quantified by spectrophotometry (NanoDrop 1000, Thermo Fisher, Waltham, MA).
683 Transcription and expression were investigated in pools of NEJs and in individual adult flukes
684 after normalization with the controls.

685 **Quantitative real-time PCR**

686 cDNA was synthesized from DNase I-treated-total RNA (10 ng) using Maxima First Strand
687 cDNA synthesis with a DNase kit (Thermo Scientific) prior to performing quantitative real-time
688 PCR (qPCR). Each cDNA sample was prepared for qPCR in triplicate using SSoAdvanced
689 Universal SYBR Green Supermix (Bio-Rad). Each qPCR reaction consisted of 5 µl of SYBR
690 Green Supermix, 0.2 µl (10 µM) each of specific forward and reverse primers for *Ov-grn-1*
691 (forward primer, *Ov*-GRN-1-RT-F: 5'-GACTTGTTGTCGCGGCTTAC-3' and reverse
692 primer, *Ov*-GRN1-RT-R: 5'-CGCGAAAGTAGCTTGTGGTC-3'), amplifying 147 base pairs
693 (bp) of 444 nt of *Ov-grn-1* mRNA, complete cds GenBank FJ436341.1) or primers for *Ov-tsp-2*
694 (forward primer, *Ov-TSP-2*-F 5'- ACAAGTCGTATGTGGAATCA- 3' and reverse primer *Ov-*
695 *TSP-2*-R 5'- CCGTCTCGCCTTCTCCTTT- 3', product size 377 bp of 672 nt of *Ov-tsp-2*A
696 mRNA, complete cds (GenBank JQ678707.1), 2 µl of cDNA and distilled water to a final
697 volume of 10 µl were used in the reaction. The thermal cycle was a single initiation cycle at
698 95°C for 10 min followed by 40 cycles of denaturation at 95°C for 15s, annealing at 55°C for 30s
699 using CFX Connect Real-Time PCR system (Bio-Rad). The endogenous actin gene (1301 nt of
700 *Ov-actin* mRNA, GenBank EL620339.1) was used as a reference [18, 57, 58] (forward
701 primer, *Ov*-actin-F: 5'-AGCCAACCGAGAGAAGATGA and reverse primer, *Ov*-actin-R: 5'-
702 ACCTGACCATCAGGCAGTTC. The fold change in *Ov-grn-1* and *Ov-tsp*-2 transcripts was
703 calculated using the $2^{(-\Delta\Delta Ct)}$ method using the *Ov-actin* gene as a reference for normalization [18,
704 57, 58].
705
706 **Illumina based targeted next generation sequencing of targeted amplicons**
707
708 The Amplicon-EZ next generation sequencing service (GENEWIZ, South Plainfield, NJ) was
709 used to obtain deeper coverage of the exon 1 from individual mature worms or pooled NEJ,
710 providing >50,000 reads per sample. A 173 nucleotide region flanking the programmed DSB
711 was amplified with forward primer 5'-TTCGAGATTCGGTCAGCCG-3' and reverse primer 5'-
712 GCACCAACTCGCAACTTACA-3', and was sequenced directly using Illumina chemistry. The
713 CRISPR-sub web platform (http://www.rgenome.net/crispr-sub/#!) analysis with comparison
714 range 60 nt was used to screen for Cas9-mediated substitutions in the reads, with comparisons
715 among the treatment groups [59]. In addition, CRISPResso2 with 30 nt quantification window
716 [14] was employed for indel estimation, as described [7]. The NGS reads are available at
717 GenBank Bioproject PRJNA385864, BioSample SAMN07287348, SRA study PRJNA385864,
718 accessions SRR 15906234-15906251.
719
720 **BrdU-staining for proliferation of biliary epithelial cells**
721

722 Proliferation of biliary epithelial cells was investigated by using incorporation of BrdU. In brief,
723 the liver sections of a paraffin-embedded sample were soaked in xylene, rehydrated in graded
724 alcohol solution (100%, 90%, and 70% ethanol for 5 min each), and antigen was retrieved in
725 citrate buffer (pH 6) for 5 min in a high-pressure cooker. The tissue sections were blocked with
726 3% H_2O_2 in methanol for 30 min and subsequently incubated with 5% fetal bovine serum in
727 phosphate buffered saline for 30 min at room temperature (RT). The sections were incubated
728 with monoclonal mouse anti-BrdU (Abcam, catalogue no. ab8955) diluted 1:200 in PBS at 4°C
729 overnight, and then probed with goat anti-mouse IgG-HRP (Invitrogen, Thermo Fisher) diluted
730 1:1,000 in PBS for 60 min at RT. The peroxidase reaction was developed with 3, 3'-
731 diaminobenzidine (DAB). Sections were counterstained with Mayer's hematoxylin for 5 min
732 before dehydrating and mounting. A positive signal was indicated by a brown color under light
733 microscopy. The image was captured by a Zeiss Axiocam microscope camera ICc5 and NIS-
734 Element software (Nikon, Japan). To quantify BrdU-positive nuclei, cholangiocytes were
735 counted in 10 non-overlapping fields of 400x magnification, with a total of 1,000 biliary
736 cholangiocytes counted using the counter plug-in of ImageJ 1.52P. The cell proliferation index
737 was calculated as a percentage using the formula: positive biliary nuclei/total biliary cells
738 x100%.
739
740 **Immunohistochemical staining for mutant forms of p53**
741
742 To investigate levels of p53 mutation [60] in cholangiocytes, paraffin-embedded tissue sections
743 were deparaffinized and rehydrated by standard methods. Thereafter, sections were incubated
744 with monoclonal mouse anti-p53 (mutant, clone Ab-3 PAb240 catalogue no. OP29-200UG)
745 (Merck, Darmstadt, Germany) diluted 1:100 in PBS at 4°C overnight , and after thorough
746 washing, probed with goat anti-mouse IgG-HRP (Invitrogen, Carlsbad, CA) diluted 1:1,000 in
747 PBS for 60 min at 25°C. The peroxidase reaction was developed with 3,3'- DAB and sections
748 counterstained with Mayer's hematoxylin for 5 min. A human CCA cell line served as the
749 positive control for p53 positivity [61, 62]. Images of high-power fields (400x magnification) of
750 the biliary epithelium were taken in five non-overlapping fields of each of the right, middle, and
751 left liver lobes using a Zeiss Axiocam fitted with a ICc5 camera and NIS-Element software
752 (Nikon). The percentage of mutant p53-positive cholangiocytes was determined by calculating
753 positive cells from 500 to 800 cholangiocytes from the right, middle, and left lobes of the liver
754 using imageJ.
755
756 **PSR staining for fibrosis evaluation**
757
758 Liver tissue sections where *O. viverrini* reside were selected for fibrosis measurements with PSR
759 (Abcam, catalogue ab150681). The thin sections were deparaffinized in xylene and rehydrated
760 through an ethanol gradient. PSR solution was applied to the sections and incubated at 25°C for
761 60 min. Excess dye was removed by washing twice in dilute acetic acid (0.5%) after which
762 sections were dehydrated through graded series of ethanol and xylene, the slides cleared with
763 100% xylene, mounted in Per-mount, and air dried overnight. Fibrosis around the bile duct
764 (periductal fibrosis, PF) proximal to the liver flukes was evaluated by two approaches: first, by
765 scoring according to accepted criteria [17, 55]. Samples were blinded and fibrosis scores (0-6)
766 were graded semi-quantitatively by Ishak stage (Table 1) by two experienced pathologists.
767 Second, localized fibrosis was evaluated by capturing images for quantification of collagen

768 deposition. Specifically, the PSR-stained fibrotic lesions was measured using the plug-in fibrosis
769 tool developed by Volker Bäcker (New FUJI toolsets for bioimage analysis,
770 DOI:10.13140/RG.2.2.15064.60167, available at
771 https://github.com/MontpellierRessourcesImagerie/imagej_macros_and_scripts/wiki/MRI_Fibro
772 sis_Tool. Others [63, 64] and we [7] have used this tool with PSR-stained tissues.
773
774 **Statistical analysis**
775
776 One-way ANOVA with Tukey multiple comparisons was used for comparisons with 2-4
777 replicates (NEJ transcripts, worm burden, 14 week EPG). The Krustal-Wallis non parametric
778 test with Dunn's multiple comparisons was used for datasets that were not normally distributed
779 including transcripts in adult liver flukes at weeks 14 and 24, 24-week EPGs, Ishak and
780 periductal fibrosis, BrdU, and anti-mutant p53 signals. Replicates are shown with the mean and
781 standard error of the mean (x±SEM) bars or as median with interquartile ranges for non-normal
782 distributions. Statistical analysis and graphic presentation of the results were undertaken using
783 GraphPad Prism version 9 (GraphPad Software Inc, San Diego, CA). As indel % values did not
784 have replicates for the SCR group, a one sample *t* test for either NEJs or adult *O. viverrini* worms
785 comparing values for the *ΔOv-grn-1* and the corresponding SCR group was used. The
786 correlation between % indel and transcript levels was assessed using a two-tailed non-parametric
787 Spearman correlation co-efficient (r_s). Values of $P \leq 0.05$ were considered to be statistically
788 significant; the asterisks (*) correspond to the SCR vs *ΔOv-grn-1* group comparisons; *, *P*0.05,
789 **, $P \leq 0.01$, ***, $P \leq 0.001$, ****, $P \leq 0.0001$; hashes (#) to *ΔOv-grn-1* vs *ΔOv-tsp-2* group
790 comparisons; #, $P \leq 0.05$; ##, $P \leq 0.01$; ###, $P \leq 0.00$; ####, $P \leq 0.0001$.
791
792 **Acknowledgements**
793
794 We thank Suwit Balthaisong for technical assistance. This study was supported by the Research
795 Program, Research and Graduate Studies, Khon Kaen University to SC, ST and TL), the
796 National Cancer Institute, National Institutes of Health (NIH) USA award R01CA164719 (AL,
797 TL, PJB,) and the Australian National Health and Medical Research Council (NHMRC award
798 APP1085309 to AL, JS and TL, and senior principal research fellowship APP1117504 to AL).
799 This research was funded in part, by the Wellcome Trust (WT), grant number
800 107475/Z/15/Z. For the purpose of Open Access, the authors have applied a CC BY public
801 copyright license to any Author Accepted Manuscript version arising from this submission. The
802 content is solely the responsibility of the authors and does not necessarily represent the official
803 views of the NCI, NIH, NHMRC, or WT.
804
805 **Author contributions**
806
807 T. Laha, A. Loukas, P. Brindley, S. Tangkawattana, S. Chaiyadet, W. Ittiprasert, P. Arunsan, and
808 M. Smout conceived and designed the research; S. Chaiyadet, S. Tangkawattana, R. Deenonpoe,
809 V. Mann, M. Smout, and W. Ittiprasert performed the research; S. Chaiyadet, S. Tangkawattana,
810 R. Deenonpoe, and M. Smout recorded the findings ; T. Laha, P.J. Brindley, A. Loukas, M.
811 Smout and W. Ittiprasert contributed reagents and analytical tools; T. Laha, S. Chaiyadet, P.
812 Arunsan, S. Tangkawattana, V. Mann, M. Smout, and W. Ittiprasert completed the experiments;
813 S. Chaiyadet, S. Tangkawattana, W. Ittiprasert, and M. Smout analyzed data; S. Chaiyadet, S.

Tangkawattana, T. Laha, P. Brindley, W. Ittiprasert, M. Smout, and A. Loukas prepared figures and wrote the paper.

Author ORCiD

Wannaporn Ittiprasert, http://orcid.org/0000-0001-9411-8883
Michael J. Smout, https://orcid.org/0000-0001-6937-0112
Paul J. Brindley, https://orcid.org/0000-0003-1765-0002
Alex Loukas, https://orcid.org/0000-0002-0896-8441

Conflict of interest. The authors declare that this study was performed without any commercial or financial relationships construable as potential conflicts of interest.

827 **References**

828

829 1. Kitadokoro K, Bordo D, Galli G, Petracca R, Falugi F, Abrignani S, Grandi G, Bolognesi
830 M: **CD81 extracellular domain 3D structure: insight into the tetraspanin**
831 **superfamily structural motifs**. *EMBO J* 2001, **20**(1-2):12-18.
832 2. Brindley PJ, Bachini M, Ilyas SI, Khan SA, Loukas A, Sirica AE, Teh BT, Wongkham S,
833 Gores GJ: **Cholangiocarcinoma**. *Nat Rev Dis Primers* 2021, **7**(1):65.
834 3. IARC: **Biological agents. Volume 100 B. A review of human carcinogens**. *IARC*
835 *monographs on the evaluation of carcinogenic risks to humans* 2012, **100**(Pt B):1-441.
836 4. Brindley PJ, da Costa JM, Sripa B: **Why does infection with some helminths cause**
837 **cancer?** *Trends Cancer* 2015, **1**(3):174-182.
838 5. Smout MJ, Laha T, Mulvenna J, Sripa B, Suttiprapa S, Jones A, Brindley PJ, Loukas A:
839 **A granulin-like growth factor secreted by the carcinogenic liver fluke, Opisthorchis**
840 **viverrini, promotes proliferation of host cells**. *PLoS Pathog* 2009, **5**(10):e1000611.
841 6. Chaiyadet S, Smout M, Johnson M, Whitchurch C, Turnbull L, Kaewkes S, Sotillo J,
842 Loukas A, Sripa B: **Excretory/secretory products of the carcinogenic liver fluke are**
843 **endocytosed by human cholangiocytes and drive cell proliferation and IL6**
844 **production**. *Int J Parasitol* 2015, **45**(12):773-781.
845 7. Arunsan P, Ittiprasert W, Smout MJ, Cochran CJ, Mann VH, Chaiyadet S, Karinshak SE,
846 Sripa B, Young ND, Sotillo J *et al*: **Programmed knockout mutation of liver fluke**
847 **granulin attenuates virulence of infection-induced hepatobiliary morbidity**. *Elife*
848 2019, **8**.
849 8. Loilome W, Yongvanit P, Wongkham C, Tepsiri N, Sripa B, Sithithaworn P, Hanai S,
850 Miwa M: **Altered gene expression in Opisthorchis viverrini-associated**
851 **cholangiocarcinoma in hamster model**. *Molecular carcinogenesis* 2006, **45**(5):279-287.
852 9. Thamavit W, Kongkanuntn R, Tiwawech D, Moore MA: **Level of Opisthorchis**
853 **infestation and carcinogen dose-dependence of cholangiocarcinoma induction in**
854 **Syrian golden hamsters**. *Virchows Arch B Cell Pathol Incl Mol Pathol* 1987, **54**(1):52-
855 58.
856 10. Thamavit W, Pairojkul C, Tiwawech D, Shirai T, Ito N: **Strong promoting effect of**
857 **Opisthorchis viverrini infection on dimethylnitrosamine-initiated hamster liver**.
858 *Cancer Lett* 1994, **78**(1-3):121-125.
859 11. Sripa B, Kaewkes S, Sithithaworn P, Mairiang E, Laha T, Smout M, Pairojkul C,
860 Bhudhisawasdi V, Tesana S, Thinkamrop B *et al*: **Liver fluke induces**
861 **cholangiocarcinoma**. *PLoS Med* 2007, **4**(7):e201.
862 12. Kim JH, Choi MH, Bae YM, Oh JK, Lim MK, Hong ST: **Correlation between**
863 **discharged worms and fecal egg counts in human clonorchiasis**. *PLoS Negl Trop Dis*
864 2011, **5**(10):e1339.
865 13. Elkins DB, Sithithaworn P, Haswell-Elkins M, Kaewkes S, Awacharagan P,
866 Wongratanacheewin S: **Opisthorchis viverrini: relationships between egg counts,**
867 **worms recovered and antibody levels within an endemic community in northeast**
868 **Thailand**. *Parasitology* 1991, **102 Pt 2**:283-288.
869 14. Clement K, Rees H, Canver MC, Gehrke JM, Farouni R, Hsu JY, Cole MA, Liu DR,
870 Joung JK, Bauer DE *et al*: **CRISPResso2 provides accurate and rapid genome editing**
871 **sequence analysis**. *Nat Biotechnol* 2019, **37**(3):224-226.

872 15. Hwang G-H, Yu J, Yang S, Son WJ, Lim K, Kim HS, Kim J-S, Bae S: **CRISPR-sub:**
873 **Analysis of DNA substitution mutations caused by CRISPR-Cas9 in human cells**.
874 *Computational and Structural Biotechnology Journal* 2020, **18**:1686-1694.
875 16. Shimonishi T, Sasaki M, Nakanuma Y: **Precancerous lesions of intrahepatic**
876 **cholangiocarcinoma**. *J Hepatobiliary Pancreat Surg* 2000, **7**(6):542-550.
877 17. Goodman ZD: **Grading and staging systems for inflammation and fibrosis in chronic**
878 **liver diseases**. *J Hepatol* 2007, **47**(4):598-607.
879 18. Papatpremsiri A, Smout MJ, Loukas A, Brindley PJ, Sripa B, Laha T: **Suppression of**
880 **Ov-grn-1 encoding granulin of Opisthorchis viverrini inhibits proliferation of**
881 **biliary epithelial cells**. *Exp Parasitol* 2015, **148**:17-23.
882 19. Smout MJ, Sotillo J, Laha T, Papatpremsiri A, Rinaldi G, Pimenta RN, Chan LY,
883 Johnson MS, Turnbull L, Whitchurch CB *et al*: **Carcinogenic Parasite Secretes Growth**
884 **Factor That Accelerates Wound Healing and Potentially Promotes Neoplasia**. *PLoS*
885 *Pathog* 2015, **11**(10):e1005209.
886 20. Haugen B, Karinshak SE, Mann VH, Popratiloff A, Loukas A, Brindley PJ, Smout MJ:
887 **Granulin Secreted by the Food-Borne Liver Fluke Opisthorchis viverrini Promotes**
888 **Angiogenesis in Human Endothelial Cells**. *Front Med (Lausanne)* 2018, **5**:30.
889 21. Bansal PS, Smout MJ, Wilson D, Cobos Caceres C, Dastpeyman M, Sotillo J, Seifert J,
890 Brindley PJ, Loukas A, Daly NL: **Development of a Potent Wound Healing Agent**
891 **Based on the Liver Fluke Granulin Structural Fold**. *J Med Chem* 2017, **60**(10):4258-
892 4266.
893 22. Jusakul A, Cutcutache I, Yong CH, Lim JQ, Huang MN, Padmanabhan N, Nellore V,
894 Kongpetch S, Ng AWT, Ng LM *et al*: **Whole-Genome and Epigenomic Landscapes of**
895 **Etiologically Distinct Subtypes of Cholangiocarcinoma**. *Cancer Discov* 2017,
896 **7**(10):1116-1135.
897 23. Banales JM, Marin JJG, Lamarca A, Rodrigues PM, Khan SA, Roberts LR, Cardinale V,
898 Carpino G, Andersen JB, Braconi C *et al*: **Cholangiocarcinoma 2020: the next horizon**
899 **in mechanisms and management**. *Nature Reviews Gastroenterology & Hepatology*
900 2020, **17**(9):557-588.
901 24. Petney TN, Andrews RH, Saijuntha W, Wenz-Mucke A, Sithithaworn P: **The zoonotic,**
902 **fish-borne liver flukes Clonorchis sinensis, Opisthorchis felineus and Opisthorchis**
903 **viverrini**. *Int J Parasitol* 2013, **43**(12-13):1031-1046.
904 25. Mitacek EJ, Brunnemann KD, Suttajit M, Martin N, Limsila T, Ohshima H, Caplan LS:
905 **Exposure to N-nitroso compounds in a population of high liver cancer regions in**
906 **Thailand: volatile nitrosamine (VNA) levels in Thai food**. *Food Chem Toxicol* 1999,
907 **37**(4):297-305.
908 26. Sripa B, Tangkawattana S, Laha T, Kaewkes S, Mallory FF, Smith JF, Wilcox BA:
909 **Toward integrated opisthorchiasis control in northeast Thailand: the Lawa project**.
910 *Acta Trop* 2015, **141**(Pt B):361-367.
911 27. Lvova MN, Tangkawattana S, Balthaisong S, Katokhin AV, Mordvinov VA, Sripa B:
912 **Comparative histopathology of Opisthorchis felineus and Opisthorchis viverrini in a**
913 **hamster model: an implication of high pathogenicity of the European liver fluke**.
914 *Parasitol Int* 2012, **61**(1):167-172.
915 28. Kim E, Hart T: **Improved analysis of CRISPR fitness screens and reduced off-target**
916 **effects with the BAGEL2 gene essentiality classifier**. *Genome Med* 2021, **13**(1):2.

917 29. Chai AWY, Yee PS, Price S, Yee SM, Lee HM, Tiong VK, Goncalves E, Behan FM,
918 Bateson J, Gilbert J *et al*: **Genome-wide CRISPR screens of oral squamous cell**
919 **carcinoma reveal fitness genes in the Hippo pathway**. *Elife* 2020, **9**.
920 30. Chaiyadet S, Krueajampa W, Hipkaeo W, Plosan Y, Piratae S, Sotillo J, Smout M, Sripa
921 B, Brindley PJ, Loukas A *et al*: **Suppression of mRNAs encoding CD63 family**
922 **tetraspanins from the carcinogenic liver fluke Opisthorchis viverrini results in**
923 **distinct tegument phenotypes**. *Sci Rep* 2017, **7**(1):14342.
924 31. International Helminth Genomes C: **Comparative genomics of the major parasitic**
925 **worms**. *Nat Genet* 2019, **51**(1):163-174.
926 32. Sripa B, Brindley PJ, Mulvenna J, Laha T, Smout MJ, Mairiang E, Bethony JM, Loukas
927 A: **The tumorigenic liver fluke Opisthorchis viverrini--multiple pathways to cancer**.
928 *Trends Parasitol* 2012, **28**(10):395-407.
929 33. Sripa B, Tangkawattana S, Sangnikul T: **The Lawa model: A sustainable, integrated**
930 **opisthorchiasis control program using the EcoHealth approach in the Lawa Lake**
931 **region of Thailand**. *Parasitol Int* 2017, **66**(4):346-354.
932 34. Fedorova OS, Fedotova MM, Zvonareva OI, Mazeina SV, Kovshirina YV, Sokolova TS,
933 Golovach EA, Kovshirina AE, Konovalova UV, Kolomeets IL *et al*: **Opisthorchis**
934 **felineus infection, risks, and morbidity in rural Western Siberia, Russian**
935 **Federation**. *PLoS Negl Trop Dis* 2020, **14**(6):e0008421.
936 35. Chan-On W, Nairismagi ML, Ong CK, Lim WK, Dima S, Pairojkul C, Lim KH,
937 McPherson JR, Cutcutache I, Heng HL *et al*: **Exome sequencing identifies distinct**
938 **mutational patterns in liver fluke-related and non-infection-related bile duct**
939 **cancers**. *Nat Genet* 2013, **45**(12):1474-1478.
940 36. Ong CK, Subimerb C, Pairojkul C, Wongkham S, Cutcutache I, Yu W, McPherson JR,
941 Allen GE, Ng CC, Wong BH *et al*: **Exome sequencing of liver fluke-associated**
942 **cholangiocarcinoma**. *Nat Genet* 2012, **44**(6):690-693.
943 37. Chaisaingmongkol J, Budhu A, Dang H, Rabibhadana S, Pupacdi B, Kwon SM, Forgues
944 M, Pomyen Y, Bhudhisawasdi V, Lertprasertsuke N *et al*: **Common Molecular**
945 **Subtypes Among Asian Hepatocellular Carcinoma and Cholangiocarcinoma**.
946 *Cancer Cell* 2017, **32**(1):57-70 e53.
947 38. Montal R, Sia D, Montironi C, Leow WQ, Esteban-Fabro R, Pinyol R, Torres-Martin M,
948 Bassaganyas L, Moeini A, Peix J *et al*: **Molecular classification and therapeutic**
949 **targets in extrahepatic cholangiocarcinoma**. *J Hepatol* 2020, **73**(2):315-327.
950 39. Frangoul H, Altshuler D, Cappellini MD, Chen YS, Domm J, Eustace BK, Foell J, de la
951 Fuente J, Grupp S, Handgretinger R *et al*: **CRISPR-Cas9 Gene Editing for Sickle Cell**
952 **Disease and β-Thalassemia**. *N Engl J Med* 2021, **384**(3):252-260.
953 40. Fellmann C, Gowen BG, Lin PC, Doudna JA, Corn JE: **Cornerstones of CRISPR-Cas**
954 **in drug discovery and therapy**. *Nat Rev Drug Discov* 2017, **16**(2):89-100.
955 41. Chaiyarit P, Sithithaworn P, Thuwajit C, Yongvanit P: **Detection of salivary antibodies**
956 **to crude antigens of Opisthorchis viverrini in opisthorchiasis and**
957 **cholangiocarcinoma patients**. *Clin Oral Investig* 2011, **15**(4):477-483.
958 42. Phumrattanaprapin W, Chaiyadet S, Brindley PJ, Pearson M, Smout MJ, Loukas A, Laha
959 T: **Orally Administered Bacillus Spores Expressing an Extracellular Vesicle-Derived**
960 **Tetraspanin Protect Hamsters Against Challenge Infection With Carcinogenic**
961 **Human Liver Fluke**. *J Infect Dis* 2021, **223**(8):1445-1455.

962 43. Pinlaor S, Onsurathum S, Boonmars T, Pinlaor P, Hongsrichan N, Chaidee A, Haonon O,
963 Limviroj W, Tesana S, Kaewkes S *et al*: **Distribution and abundance of Opisthorchis**
964 **viverrini metacercariae in cyprinid fish in Northeastern Thailand**. *The Korean*
965 *journal of parasitology* 2013, **51**(6):703-710.
966 44. Ran FA, Hsu PD, Wright J, Agarwala V, Scott DA, Zhang F: **Genome engineering**
967 **using the CRISPR-Cas9 system**. *Nature Protocols* 2013, **8**(11):2281-2308.
968 45. Montague TG, Cruz JM, Gagnon JA, Church GM, Valen E: **CHOPCHOP: a**
969 **CRISPR/Cas9 and TALEN web tool for genome editing**. *Nucleic Acids Research*
970 2014, **42**(W1):W401-W407.
971 46. Labun K, Montague TG, Gagnon JA, Thyme SB, Valen E: **CHOPCHOP v2: a web tool**
972 **for the next generation of CRISPR genome engineering**. *Nucleic Acids Research*
973 2016, **44**(W1):W272-W276.
974 47. Young ND, Nagarajan N, Lin SJ, Korhonen PK, Jex AR, Hall RS, Safavi-Hemami H,
975 Kaewkong W, Bertrand D, Gao S *et al*: **The Opisthorchis viverrini genome provides**
976 **insights into life in the bile duct**. *Nat Commun* 2014, **5**:4378.
977 48. Laha T, Pinlaor P, Mulvenna J, Sripa B, Sripa M, Smout MJ, Gasser RB, Brindley PJ,
978 Loukas A: **Gene discovery for the carcinogenic human liver fluke, Opisthorchis**
979 **viverrini**. *BMC Genomics* 2007, **8**:189.
980 49. Hulme BJ, Geyer KK, Forde-Thomas JE, Padalino G, Phillips DW, Ittiprasert W,
981 Karinshak SE, Mann VH, Chalmers IW, Brindley PJ *et al*: **Schistosoma**
982 **mansoni α-N-acetylgalactosaminidase (SmNAGAL) regulates coordinated**
983 **parasite movement and egg production**. *bioRxiv* 2021:2021.2007.2026.453800.
984 50. Suyapoh W, Tangkawattana S, Suttiprapa S, Punyapornwithaya V, Tangkawattana P,
985 Sripa B: **Synergistic effects of cagA+ Helicobacter pylori co-infected with**
986 **Opisthorchis viverrini on hepatobiliary pathology in hamsters**. *Acta Tropica* 2021,
987 **213**:105740.
988 51. Zen Y, Adsay NV, Bardadin K, Colombari R, Ferrell L, Haga H, Hong SM, Hytiroglou
989 P, Kloppel G, Lauwers GY *et al*: **Biliary intraepithelial neoplasia: an international**
990 **interobserver agreement study and proposal for diagnostic criteria**. *Modern*
991 *pathology : an official journal of the United States and Canadian Academy of Pathology,*
992 *Inc* 2007, **20**(6):701-709.
993 52. Sato Y, Sasaki M, Harada K, Aishima S, Fukusato T, Ojima H, Kanai Y, Kage M,
994 Nakanuma Y, Tsubouchi H: **Pathological diagnosis of flat epithelial lesions of the**
995 **biliary tract with emphasis on biliary intraepithelial neoplasia**. *J Gastroenterol* 2014,
996 **49**(1):64-72.
997 53. Sudsarn P, Boonmars T, Ruangjirachuporn W, Namwat N, Loilome W, Sriraj P,
998 Aukkanimart R, Nadchanan W, Jiraporn S: **Combination of Praziquantel and Aspirin**
999 **Minimizes Liver Pathology of Hamster Opisthorchis viverrini Infection Associated**
1000 **Cholangiocarcinoma**. *Pathol Oncol Res* 2016, **22**(1):57-65.
1001 54. Sudsarn P, Wongchalee N, Boonmars T, Laummaunwai P, Chamgramol Y, Pairojkul C,
1002 Juasook A, Boonjaraspinyo S: **Sex differences in opisthorchiosis and the development**
1003 **of cholangiocarcinoma in Syrian hamster model**. *Parasitol Res* 2014, **113**(3):829-835.
1004 55. Ishak K, Baptista A, Bianchi L, Callea F, De Groote J, Gudat F, Denk H, Desmet V,
1005 Korb G, MacSween RN *et al*: **Histological grading and staging of chronic hepatitis**. *J*
1006 *Hepatol* 1995, **22**(6):696-699.

1007 56. Elkins DB, Haswell-Elkins M, Anderson RM: **The epidemiology and control of**
1008 **intestinal helminths in the Pulicat Lake region of Southern India. I. Study design**
1009 **and pre- and post-treatment observations on Ascaris lumbricoides infection**. *Trans R*
1010 *Soc Trop Med Hyg* 1986, **80**(5):774-792.
1011 57. Piratae S, Tesana S, Jones MK, Brindley PJ, Loukas A, Lovas E, Eursitthichai V, Sripa
1012 B, Thanasuwan S, Laha T: **Molecular characterization of a tetraspanin from the**
1013 **human liver fluke, Opisthorchis viverrini**. *PLoS Negl Trop Dis* 2012, **6**(12):e1939.
1014 58. Schmittgen TD, Livak KJ: **Analyzing real-time PCR data by the comparative CT**
1015 **method**. *Nature Protocols* 2008, **3**(6):1101-1108.
1016 59. Hwang GH, Yu J, Yang S, Son WJ, Lim K, Kim HS, Kim JS, Bae S: **CRISPR-sub:**
1017 **Analysis of DNA substitution mutations caused by CRISPR-Cas9 in human cells**.
1018 *Comput Struct Biotechnol J* 2020, **18**:1686-1694.
1019 60. Surget S, Khoury MP, Bourdon JC: **Uncovering the role of p53 splice variants in**
1020 **human malignancy: a clinical perspective**. *Onco Targets Ther* 2013, **7**:57-68.
1021 61. Nakayama M, Oshima M: **Mutant p53 in colon cancer**. *Journal of Molecular Cell*
1022 *Biology* 2018, **11**(4):267-276.
1023 62. Batheja N, Suriawinata A, Saxena R, Ionescu G, Schwartz M, Thung SN: **Expression of**
1024 **p53 and PCNA in Cholangiocarcinoma and Primary Sclerosing Cholangitis**. *Modern*
1025 *Pathology* 2000, **13**(12):1265-1268.
1026 63. Rabacal W, Schweitzer F, Rayens E, Tarantelli R, Whang P, Jimenez VC, Outwater JA,
1027 Norris KA: **Statin treatment prevents the development of pulmonary arterial**
1028 **hypertension in a nonhuman primate model of HIV-associated PAH**. *Scientific*
1029 *Reports* 2019, **9**(1):19832.
1030 64. Hollenbach M, Thonig A, Pohl S, Ripoll C, Michel M, Zipprich A: **Expression of**
1031 **glyoxalase-I is reduced in cirrhotic livers: A possible mechanism in the development**
1032 **of cirrhosis**. *PLoS One* 2017, **12**(2):e0171260.

1033
1034
1035
1036
1037
1038
1039
1040
1041
1042
1043
1044
1045

Supporting information

Supporting information

Supplementary Figure S1: Nucleotide substitutions at targeted gene locus. Patterns of non - Cas9 mediated substitutions identified in amplicons representing the *Ov-grn-1* gene locus, in genomic DNAs from pools of newly ex-sheathed juveniles (NEJ) and single adults of *Opisthorchis viverrini* liver flukes in the *ΔOv-grn-1* treatment group compared with the control SCR group. Specifically, CRISPR-sub analysis using the online tools at http://www.rgenome.net/crispr-sub/#! revealed patterns of nucleotide substitutions in sequence reads in the experimental programmed CRISPR/Cas9 on-target edited alleles versus alleles from the control (SCR) group. Most substitutions were not mediated by CRISPR/Cas9 catalysis, as assessed using statistical analysis. The Y-axis reports the substitution rate at each position within additional flanking windows (%). The negative Y-axis shows the data for the control group (blue bars) and the positive Y-axis shows the data for the experimental group (red bars). The X-axis shows the gene target sites including the site of the programmed double stranded break (DSB), indicated as 0, and ≥ 20 nt upstream and downstream sequence flanking the programmed DSB resulting from RNA-guided CRISPR/Cas9 cleavage. Findings from the NEJs are shown at the top left and each worm is shown separately and designated with the hamster number (x), 1-15, from which the adult fluke was recovered and worm number (y), 1-3; i.e., h "x" worm "y".

Supplementary Table S1. Summary of NGS sequencing data. Frequency of CRISPR/Cas9 gene knockout as determined by frameshift mutations. Analysis by CRISPResso2 employing a window size (-3 option) that included the entire 173 bp amplicon but excluded 25 bp of the 5' and 3' terminal residues, which represented the primer binding region. To conform with the colors in the figures, the SCR groups are highlighted in blue, and the low level, medium level and highly edited adults are highlighted in red, purple and green. respectively.

Supplementary Table S2: Assessment of pre-malignant and malignant lesions. Disease outcomes in the three groups of hamsters. Whereas Figure 5 summarized the histopathological diagnoses in graphical format, the table lists histopathological cholangiocarcinoma (CCA) tumor type, tumor location, and tumor progression. Representative micrographs of major histopathological types of CCA are provided below the table: **A** = tubular; **B** = papillary; and **C** = mucinous.

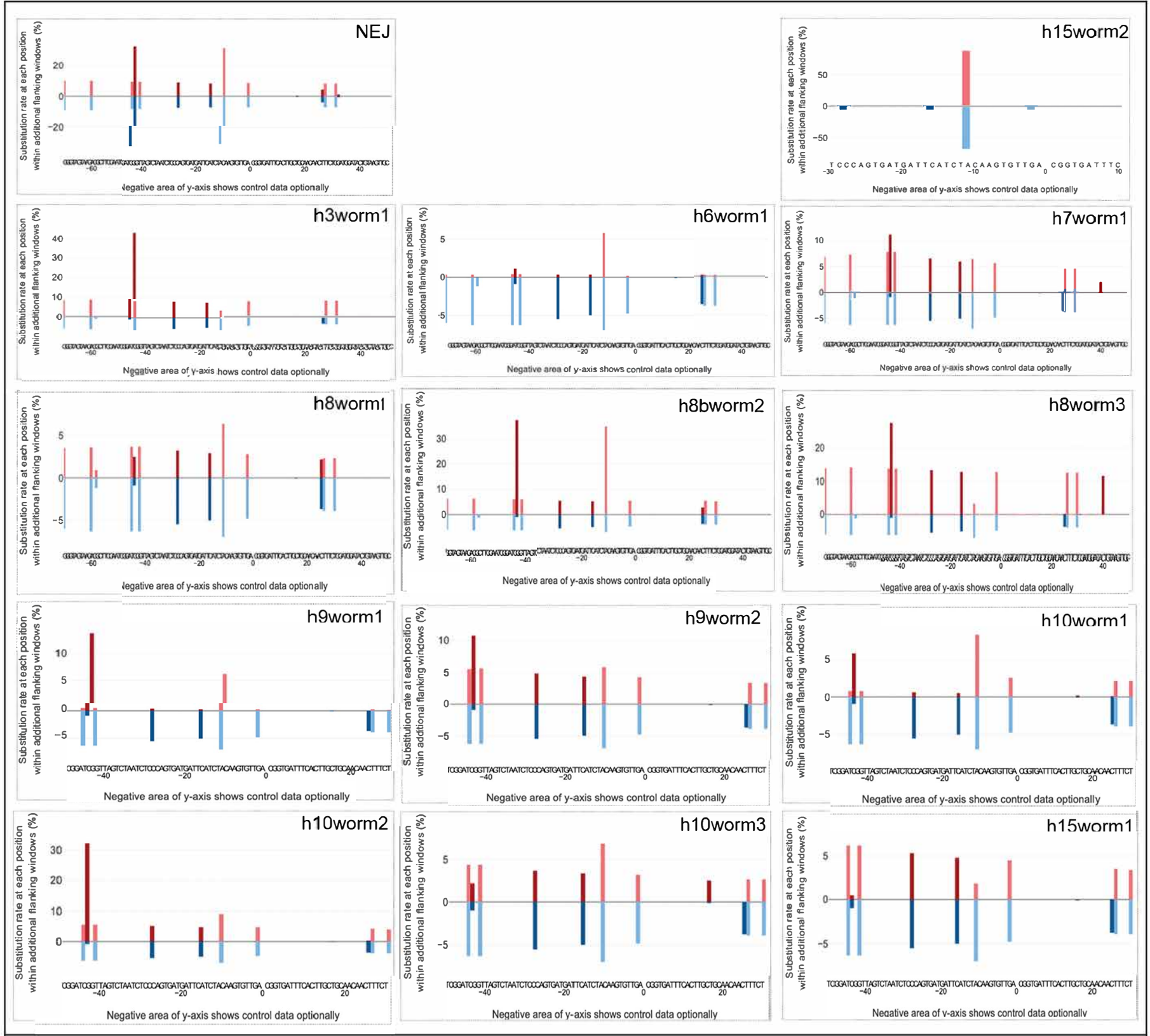
NEJ
h15worm2
h3worm1
h6worm1
h7worm1
h8worm1
h8bworm2
h8worm3
h9worm1
h9worm2
h10worm1
h10worm2
h10worm3
h15worm1
Substitution rate at each position within additional flanking windows (%)
Negative area of y-axis shows control data optionally

Figure S1

Table S1

Sample	Read-pairs sequences	Read-pairs aligned	Unmodified reads	Modified reads	Insertions	Deletions	Frameshift mutation (number,%)	Indel (%)
NEJs								
SCR NEJs	113,442	51,402	51,384	18	0	18	0	**0.035**
ΔOv-grn-1 NEJs	159,583	80,571	77,848	2,723	0	2,723	2 (0.02%)	**3.38**
ADULT FLUKES								
Hamster 1-15: SCR flukes	129,859	91,783	91,742	41	0	41	0	**0.045**
***$_L$ΔOv-grn-1* flukes (0-0.04% indels)**								
Hamster 6: fluke 1	185,269	105,363	105,363	0	0	0	0	**0.000**
Hamster 8: fluke 1	171,164	110,079	110,078	1	0	1	0	**0.001**
Hamster 3: fluke 1	150,356	60,954	60,935	19	0	19	0	**0.031**
Hamster 8: fluke 3	154,598	101,288	101,252	36	2	34	0	**0.036**
Hamster 10: fluke 1	143,186	118,253	118,211	41	0	41	19 (48.8%)	**0.036**
Hamster 9: fluke 1	193,741	168,806	168,741	65	0	65	0	**0.039**
***$_M$ΔOv-grn-1* flukes (3.1% indels)**								
Hamster 8: fluke 2	169,500	116,021	112,458	3,563	1	3,563	8 (0.20%)	**3.07**
***$_H$ΔOv-grn-1* flukes (51-91% indels)**								
Hamster 10: fluke 2	169,733	128,391	63,378	65,013	0	65,013	20 (0.03%)	**50.6**
Hamster 15: fluke 2	166,531	143,206	64,899	78,307	1	78,307	0	**54.7**
Hamster 7: fluke 2	182,260	102,168	27,617	74,551	0	74,551	0	**73.0**
Hamster 10: fluke 3	161,903	120,064	26,447	93,617	0	93,617	22 (0.02%)	**78.0**
Hamster 9: fluke 2	125,032	99,750	19,707	80,043	2	80,042	17 (0.02%)	**80.2**
Hamster 15: fluke 1	155,792	115,881	10,413	105,468	1	105,468	0	**91.0**

Table S2
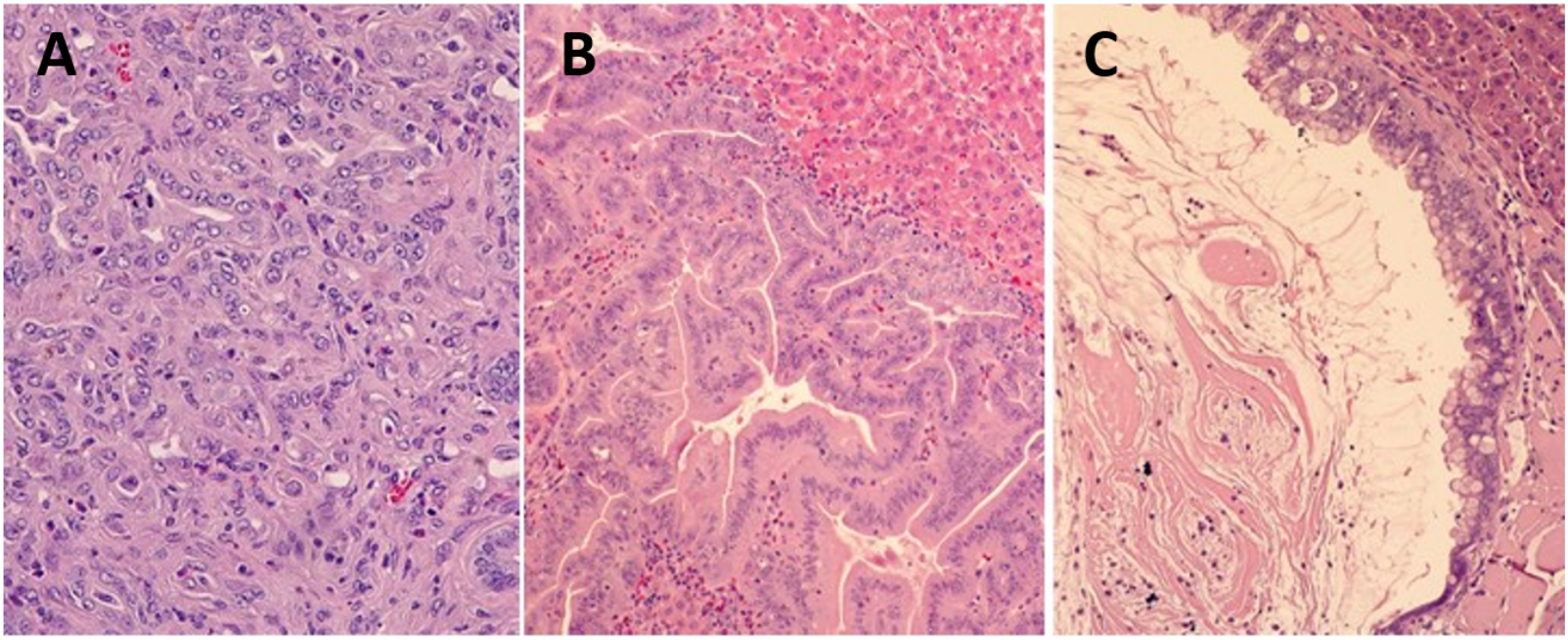
Parameters / Groups	SCR	*ΔOv-grn-1*	*ΔOv-tsp-2*
CCA development			
CCA positive hamsters/total hamsters (% positive)	10/12 (83.33%)	9/13 (69.23%)	7/13 (53.85%)
Histopathological diagnosis			
Dysplasia (precancerous lesion)	2	1	2
Low grade CCA	2	5	1
High grade CCA	8	4	6
CCA histopathological type			
Tubular	9	6	4
Papillary/Cystic	0	1	0
Mucinous	1	0	3
CCA location (lobe)			
Right	6	5	4
Left	1	2	2
Middle	0	0	1
Right and Left	2	1	0
Right and Middle	1	0	0
Right, Middle and Left	0	1	0
Tumor progression			
Focal	6	3	1
Fully developed	4	4	6